We are IntechOpen, the world's leading publisher of Open Access books
Built by scientists, for scientists

6,900
Open access books available

185,000
International authors and editors

200M
Downloads

Our authors are among the

154
Countries delivered to

TOP 1%
most cited scientists

12.2%
Contributors from top 500 universities

WEB OF SCIENCE™

Selection of our books indexed in the Book Citation Index in Web of Science™ Core Collection (BKCI)

Interested in publishing with us?
Contact book.department@intechopen.com

Numbers displayed above are based on latest data collected.
For more information visit www.intechopen.com

Chapter

Hydrogenation and Hydrogenolysis with Ruthenium Catalysts and Application to Biomass Conversion

Thomas Ernst Müller

Abstract

With the rising emphasis on efficient and highly selective chemical transformations, the field of ruthenium-catalysed hydrogenation and hydrogenolysis reactions has grown tremendously over recent years. The advances are triggered by the detailed understanding of the catalytic pathways that have enabled researchers to improve known transformations and realise new transformations in biomass conversion. Starting with the properties of ruthenium, this chapter introduces the concept of the catalytic function as a basis for rational design of ruthenium catalysts. Emphasis is placed on discussing the principles of dissociative adsorption of hydrogen. The principles are then applied to the conversion of typical biomolecules such as cellulose, hemicellulose and lignin. Characteristic features make ruthenium catalysis one of the most outstanding tools for implementing sustainable chemical transformations.

Keywords: ruthenium, catalysis, reaction network, sequential reactions, hydrogen dissociation, hydrogenation, hydrogenolysis, biomass conversion

1. Introduction

Life on earth inherently depends on the element carbon creating the heart of a myriad of chemical compounds that, together with water and some inorganic compounds, build living matter. Over geologic periods, life has established a dynamic equilibrium of the flows of carbon through the different geo-habitats [1]. With the rise of mankind, this balance has been undermined through the exploitation of vast amounts of fossil resources for generating heat and materials. The carbon dioxide (CO_2) emissions from combustion of fossil resources have resulted in rising atmospheric CO_2 concentrations and an increasingly evident change in the climate worldwide. Replacing fossil resources that at present make up more than 90% of the energy demand and the feedstock for the chemical industry [2] is one of the most pressing challenges of mankind. All our primary energy demand of annually 12.5 TW a^{-1} could be covered by harnessing a fraction of the 8405 TW a^{-1} renewable energy available annually that comprises solar, wind, geothermal, tidal and wave energy [3]. Nevertheless, a sustainable energy supply will be needed for carbon-based compounds in order to close carbon recycle streams. Biomass is a globally

available resource that is considered a suitable alternative feedstock for producing basic chemical building blocks, so-called platform molecules [4], that could substitute the current fossil-based platform chemicals [5].

Biomass largely consists of complex molecules comprising mostly oxygen and other heteroatoms. Lignocellulose, the structural component of plants and the largest fraction of plant biomass, is essentially composed of cellulose, hemicellulose and lignin. Break down of the structure by depolymerisation of the corresponding molecular entities, followed by oxygen removal, yields fuels and platform chemicals for the value-chain of the chemical industry. Sustainable conversion depends on efficient conversion steps obtained ideally via catalytic processes. In this context, the catalytically highly active element ruthenium provides unique properties. Despite ruthenium being counted among the noble metals, it resembles a non-noble metal in many aspects. In metallic form, ruthenium atoms are highly polarisable. Unlike the higher homologue platinum, e.g., that has similar atomic radius, ruthenium has a much higher average electric dipole polarizability. Consequently, distinct catalytic functions can be realised with ruthenium catalysts.

To help readers understand why ruthenium catalysts are so frequently employed in biomass conversion, this chapter will first investigate the properties of ruthenium. Here, the catalytic properties of ruthenium are linked with its propensity to adsorb certain molecular entities. After exploring the interaction of adsorbed molecules with ruthenium surfaces, we will discuss the nature of selected adsorption states, the corresponding binding energies and structures of the adsorption complexes including ordering phenomena observed for molecules co-adsorbed on the ruthenium metal surface. This sets the scene for rational design of catalysts that are specific for the conversion of chemical entities in biomass. Last but not least, we will discuss selected examples for intriguing transformations of biomolecules.

To note here is that this chapter does not aim to comprehensively review the available data on catalysis with ruthenium. Nor does it attempt to summarise all data on the conversion of biomass with ruthenium catalysts. The extensive interest in this field is reflected presently by the more than 800 articles published each year on catalysis with ruthenium, more than 110 of which focus on biomass conversion. Instead, this chapter aims to summarise the catalytic principles governing hydrogenation and hydrogenolysis reactions with heterogeneous ruthenium catalysts with particular focus on applications in biomass conversion. Cited data and papers were selected to exemplify the field and illuminate the discussion.

2. Ruthenium

Ruthenium, from Latin *ruthenia* ("Russia"), is one of the late transition metals and is located in the periodic table in the 5th period and group 8 (**Figure 1**). With an abundance of 7.0 ± 0.9 $ng \cdot g^{-1}$ in the silicate shell [6], ruthenium is one of the rarest non-radioactive elements on earth. Its low abundance is due to segregation of the platinum group elements in the core of Earth that was partially compensated by addition of 0.3–0.8% of chondritic material after core formation had been complete [6]. Ruthenium is found mostly in deposits associated with the other platinum-group elements [7] and as the rare RuS_2 mineral called laurite [8]. Ruthenium is a silvery white, extraordinarily hard and brittle metal. With a density of 12.45 $g \cdot cm^{-3}$ [9], ruthenium is the second lightest platinum group metal after palladium. In the electronics industry, it is used in devices for perpendicular recording [10], a technology applied in hard disks that enables high-density data storage on magnetic media.

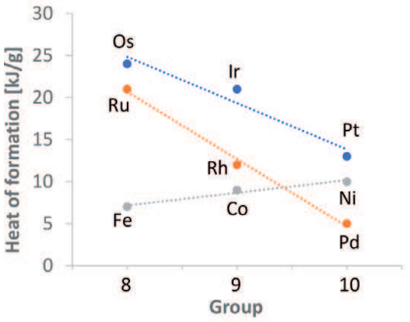

7	8	9	10	11	12
Mn	Fe	Co	Ni	**Cu**	Zn
Tc	**Ru**	**Rh**	**Pd**	**Ag**	Cd
Re	**Os**	**Ir**	**Pt**	**Au**	**Hg**

Figure 1.
Calculated heats of formation of the (unstable) binary hydrides M_nH_y ($n > y$) for group 8–10 transition metals [12] (left) and position of ruthenium (circle) in the periodic table (right) indicating the group of noble metals (bold, grey) and the platinum group metals (dark grey).

With regard to its chemical properties, ruthenium is stable in the absence of oxygen against non-oxidising acids. Consequently, it counts as a noble metal. Even so, ruthenium resembles a non-noble metal in many respects. Similar to the other metals of the 7th, 8th and 9th group of the periodic table, ruthenium does not form stable binary hydrides under ambient conditions; this region of the periodic table is called the "hydride gap" [11]. For these elements a positive value is obtained for the heats of formation calculated for the binary hydrides (**Figure 1**) [12]. Nonetheless, ruthenium monohydride (RuH) is formed by reaction of the elements at pressures above 14 GPa at room temperature. It transforms to Ru_3H_8 at pressures of more than 50 GPa and temperatures exceeding 1000 K, adopting a cubic structure, and RuH_4, when the pressure is increased above 85 GPa, crystallising in a structure comprising corner-sharing H_6 octahedra [13]. Interestingly, the hydride ligand exerts a strong *trans* influence in ruthenium complexes (*vide infra*), thereby weakening the binding of ligands located in *trans* position [14].

Due to its ability to dissociate hydrogen on the metal surface, ruthenium, in its metallic form, finds numerous applications as a catalyst in chemical processes such as ammonia synthesis, methanation, hydrogenation or hydrogenolysis (*vide infra*). Moreover, it can catalyse the oxidation of alcohols to aldehydes and carbonic acids. Ruthenium compounds are distinguished for their rich coordination chemistry, and compounds with ruthenium in oxidation states between −2 and + 8 are known. The most stable and most common oxidation states are +3 and + 4. With ruthenium at an intermediate oxidation state, +2, +3 or + 4, complexes have also been obtained that, similar to other late transition metal clusters (e.g., Ni, Pd, Pt [15]; Pt [16]; Co, Rh, Ir [17]; Au [18]), comprise ruthenium-ruthenium bonds. Ruthenium complexes, like Grubbs catalyst and Noyori catalyst (*vide infra*), play a significant role in chemical syntheses. Likewise, ruthenium compounds are employed in olefin metathesis polymerisation of cyclic alkenes [19–21]. The perovskite mixed oxide Ba_2LaRuO_6 is used in automotive exhaust gas catalysts [22]. Titanium electrodes covered with a layer of RuO_2 are applied in the chloralkaline electrolysis [23]. Moreover, ruthenium nanoparticles are interesting Deacon catalysts for the gas-phase oxidation of hydrogen chloride to chlorine [24].

3. Concept of catalytic function

At first sight, most catalytic systems appear to be unnecessarily complex. A look at biologic systems, however, reveals that many biological systems are built on chains of different catalysts. There, substrate molecules are passed from one enzyme to another. Thus, in the conversion of molecular oxygen, about ten

different catalysts are involved before the oxidising equivalents are reacted with carbon compounds [25].

Thinking in terms of sequences of consequential reaction steps is a useful strategy to rationally design heterogeneous catalysts. A good starting point is considering the catalytic functions [26] necessary for realising the desired transformations. The dissociative adsorption of molecular hydrogen is one of the key steps for hydrogenation and hydrogenolysis reactions, the focus of this chapter. In the case of transfer hydrogenation, the concepts equally apply to suitable hydrogen surrogates. As such, dissociative adsorption of hydrogen, as one of the important steps of catalysis, will be elucidated below. With the Langmuir-Hinshelwood mechanism most prominent in catalysis with late transition metals, co-adsorption of the substrate and transfer of hydrogen atoms to an unsaturated substrate need to be considered next. Other catalytic functions important for biomass conversion are the ability of a catalyst to either cleave or form C-C, C-O or C-N bonds. This results in a list of complementary catalytic functions that are required for realising the desired transformation. Thereby it is useful to consider orthogonal catalytic functions that do not interfere with each other. Rather molecules ought to be passed from one catalytic function to the next, like in a molecular assembly line. Noteworthy, such assembly lines may involve a single material comprising different functions. Frequently the support plays an important role even when the actual transformation occurs on supported metal nanoparticles. One aspect to be considered regarding hydrogenation and hydrogenolysis reactions is spill-over of hydrogen to surface sites on the support. Another concept for realising such assembly lines involve mechanical mixtures of two or more materials that comprise different catalytic functions. An example is given below. Whereas heterogeneous ruthenium catalysts can accommodate many of these catalytic functions, homogeneous ruthenium catalysts enable unique, highly distinct catalytic transformations. Once the necessary catalytic functions have been identified, it is useful to derive the link to the desired active state and the structure of the pre-catalysts that is to be used. This provides a straightforward path for rationally designing a particular catalyst for the desired transformation.

4. Sequential reactions

Rational and straight-forward catalyst design is the foundation of systematic conceptualisation of highly active catalysts that provide extraordinary specificity for a given transformation. Such specificity is essential upon designing catalysts for biomass transformations, because the chemist typically encounters many different molecules or molecular entities rather than single types of molecules that are to be converted. If chosen in the appropriate way, the catalyst will adsorb and convert only one type of molecule or chemical entity while leaving all other molecules and chemical entities untouched. This concept is also valuable for devising catalysts for sequentially connected, mutually exclusive catalytic reactions.
To develop such catalysts, the chemist needs to fundamentally understand the nature and catalytic role of active sites to guide the design of new and improved catalysts. Two examples are described here. The general principle is exemplified for a radical reaction with a MOF catalyst; the potential is then demonstrated for the hydrogenation of a multifunctional substrate over a Ru/CNT-Pt/CNT catalyst mixture.

Metal organic framework (MOF) compounds are porous materials commonly obtained by hydrothermal reaction of metal ions and bridging organic

ligands [27]. MOFs combine the high porosity of a heterogeneous catalyst with the tunability of molecular functional groups. This combination of features has been exploited for the sequential oxidation of alcohols to carboxylic acids with molecular oxygen in the presence of TEMPO modified MOF UiO-68 [28]. The conversion involves two sequential oxidation steps, i.e., the aerobic oxidation of alcohols to aldehydes, and the consequential autoxidation of the aldehydes to carboxylic acids. Whereas the first step is a radical reaction, the second step is inhibited by radicals. Thus, the two reactions are mutually exclusive. Complete removal of the MOF catalyst after the first radical-catalysed aerobic oxidation step by filtration provides the radical scavenger-free conditions that are necessary for the second radical-inhibited autoxidation step. This is a beautiful example of the use of a functional heterogeneous catalyst for a sequential organic transformation.

The concept of connecting consecutive one-pot reactions with a "molecular assembly line" has been explored for the hydrogenation of bifunctional substrates A-B to products A^H-B^H [29]. Two catalysts were chosen in such a way that one catalyst (M^1) preferentially adsorbs one of the substrate moieties, and the other catalyst (M^2) preferentially adsorbs the second substrate moiety (**Figure 2**). In this case both catalysts function optimally, thereby yielding improved rates and selectivities compared to single or conventional bimetallic catalysts [29]. Moreover, substrate inhibition can be avoided. By adjusting the relative quantity of the two catalysts, the relative rates of the two sequential transformations can be adjusted to be equal, because this results in the highest overall rate at the lowest catalyst concentration.

This concept has been applied successfully to the full hydrogenation of nitroaromatics to cycloaliphatic amines over a mechanical mixture of carbon nanotube (CNT)-supported Ru/CNT - Pt/CNT catalysts [29]. Noteworthy is that the aromatic ring, considered to be "soft" due to the aromatic π-system delocalised over six carbon atoms, preferentially adsorbs on ruthenium that is readily polarizable. The nitro group, considered to be "hard" due to the negative charge which is delocalised over only two oxygen atoms, preferentially adsorbs on platinum with highly shielded d-electrons. Notably, metallic Ru and Pt have similar atomic radii of 133 and 137 pm, while differing in the static average electric dipole polarizability of 9.6 and 6.4 10^{-24} cm^3, respectively. A 95:5 mixture of the Ru/CNT (M^1) and Pt/CNT (M^2) catalysts provides the required equal rates for hydrogenation of the two respective moieties and optimum selectivity to the target product cyclohexylamine (**Figure 3**).

		Affinity	
		M^1	**M^2**
Substrate	A-B	High	Low
Intermediate	A^H-B	Low	High
Product	A^H-B^H	Low	Low

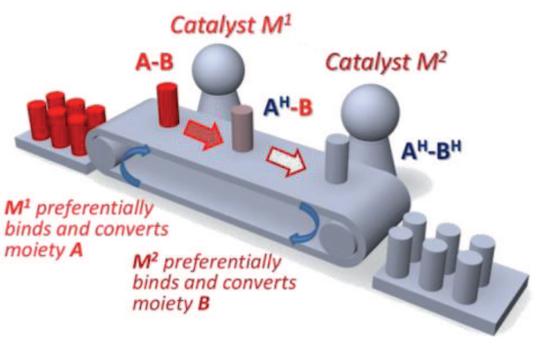

Figure 2.
Concept of a molecular assembly line for catalysing the consecutive one-pot reaction of a bifunctional subtract A-B to product a^H-B^H with a mixture of orthogonal catalysts M^1 and M^2 (right) and requirements concerning the affinity for binding of the respective moieties to the metal centres M^1 and M^2 (table, left).

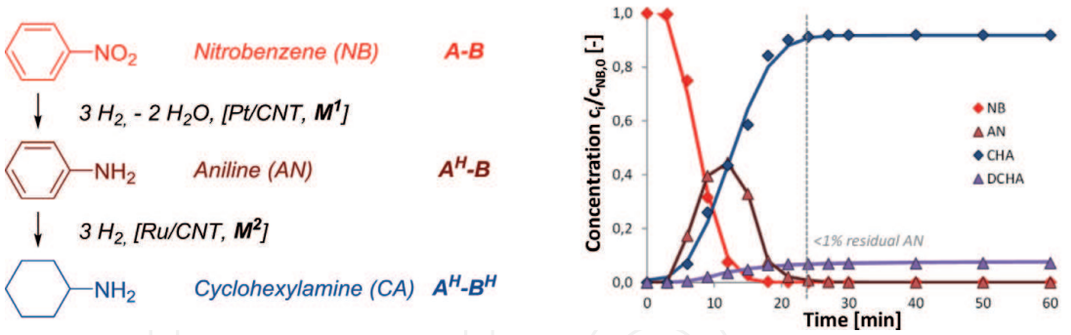

Figure 3.
Concept of a molecular assembly line applied to the hydrogenation of nitrobenzene (NB, A-B, blue) to cyclohexylamine (CA, a^H-B^H, brown) over a mixture of orthogonal catalysts Pt/CNT (M^1) and Ru/CNT (M^2) and time-concentration profile showing also the intermediate aniline (AN, A^H-B, green) and the side product dicyclohexylamine (DA, purple) (right).

5. Catalytic transformations with ruthenium catalysts

Based on the unique catalytic functions given by heterogeneous and homogeneous ruthenium catalysts, a large number of important transformations have been realised. Many of these transformations are applied on an industrial scale. For hydrogenation and hydrogenolysis reactions, in particular, heterogeneous ruthenium catalysts are among the most frequently applied catalysts, because they provide outstanding activities and excellent selectivities.

5.1 Ammonia synthesis and methanation with ruthenium catalysts

Analogous to iron and osmium, ruthenium catalyses the formation of ammonia from nitrogen and hydrogen (Eq. 1). Ruthenium has superior catalytic activity compared to iron [30] and results in enhanced NH_3 yields at lower pressures. A ruthenium catalyst, which is supported on a carbon matrix and improved by barium and caesium as promoters, has been in industrial use in two production sites in Trinidad since 1998 [31]. As the slow methanation of the carbon support [32] interferes with the process, alternative supports are preferred for ruthenium catalysts applied in ammonia synthesis. Efficiencies as close as possible to the theoretical limit are highly relevant for decentralised, islanded ammonia production plants [33, 34], where round-trip efficiencies of up to 61% can be reached [35]. An example for a highly active and stable low-temperature ammonia catalyst are ruthenium nanoparticles on a Ba-$Ca(NH_2)_2$ support [36]. At a weight hourly space velocity (WHSV) of 36 L g^{-1} h^{-1}, a rate of 23.3 $mmol_{NH3}$ g^{-1} h^{-1} is obtained at 300 °C and 9 bar. Such catalytic activity is about 6 times higher than that of industrial iron-based benchmark catalysts (at 340 °C) and 100 times higher than that of industrial ruthenium-based benchmark catalysts (Cs-doped Ru/MgO, at 260 °C) [36]. In addition, for the reverse reaction of ammonia cleavage, high activities are likewise important [37, 38] and imply the use of ruthenium catalysts for the upcoming production of CO_x-free hydrogen by ammonia cleavage in energy applications.

$$N_2 + 3H_2 \rightleftarrows 2NH_3 \quad \rightarrow \quad \Delta H_r° = -91.8\,kJ\,mol^{-1} \qquad (1)$$

Analogous to nickel, ruthenium catalyses methanation, the production of methane from hydrogen and carbon dioxide (Eq. 2) or carbon monoxide (Eq. 3), the so-called Sabatier reaction. Water is obtained as by-product. Carbon dioxide

methanation could be seen as the combination of the reverse water gas shift reaction that converts a mixture of carbon dioxide and hydrogen to carbon monoxide and water (Eq. 4), and methanation. Over ruthenium catalysts, such as Ru/Al_2O_3, the coproduction of CO is negligible [39]. This suggests a different reaction pathway not involving the intermediate formation of CO. Both reactants, H_2 and CO_2, are strongly adsorbed on the surface [39] giving rise to a Langmuir-Hinshelwood mechanism. Ruthenium catalysts are highly selective to methane and provide a very low fraction of side products, such as higher hydrocarbons, alcohols, or formic acid. Due to the exothermicity and volume reduction, the reaction is thermodynamically favoured at low temperatures and high pressures. Typical operation conditions are 200–500 °C and pressures of 10–30 bar [40]. Since ruthenium catalysts have a higher activity than nickel catalysts, they enable higher conversions at low temperature. Methanation has long been used for removing CO_x from the hydrogen-nitrogen syngas mixture used in ammonia production [41]. Carbon dioxide methanation is an option for biogas upgrading that constitutes an alternative to the removal of carbon dioxide [42]. Carbon dioxide methanation has also been discussed in the context of storing intermittent energy generated as a result of electricity production from renewable resources. Methane can be transported and stored in the existing natural gas grid. Therefore, methanation of carbon dioxide is being discussed as one of the promising Power-to-X technologies [43].

$$CO_2 + 4\ H_2 \rightleftarrows CH_4 + 2\ H_2O \quad \rightarrow \quad \Delta H_r^\circ = -165.12\ \text{kJ mol}^{-1} \tag{2}$$

$$CO + 3\ H_2 \rightleftarrows CH_4 + H_2O \quad \rightarrow \quad \Delta H_r^\circ = -206.28\ \text{kJ mol}^{-1} \tag{3}$$

$$CO_2 + H_2 \rightleftarrows CO + H_2O \quad \rightarrow \quad \Delta H_r^\circ = +41.16\ \text{kJ mol}^{-1} \tag{4}$$

5.2 Hydrogenation with ruthenium catalysts

Ruthenium is an efficient catalyst for hydrogenating aromatics, acids, ketones and unsaturated nitrogen compounds. The selective hydrogenation of aromatic amines to cycloaliphatic primary amines is an industrially relevant transformation, but is impaired by formation of secondary amines and other side products. Modification of carbon nanotube (CNT)-supported ruthenium catalysts Ru/CNT catalysts with a base (LiOH) significantly improves selectivity in toluidine hydrogenation [44, 45] without decreasing the activity of the catalysts. LiOH-modified Ru/CNT catalysts can efficiently convert also other challenging substrates, such as methylnitrobenzenes [46]. The effect of LiOH is understood as (i) LiOH reducing acidic sites on the catalyst support, (ii) enhancing hydrogen dissociation and reducing hydrogen spillover from ruthenium to the support (*vide infra*) and (iii) shifting the adsorption mode of the substrate on the ruthenium metal nanoparticles from binding of the amine group to the aromatic ring. In a similar manner, nitro compounds are able to change the binding mode of aromatic amines to the ruthenium surface [47, 48].

5.3 Hydrogenolysis with ruthenium catalysts

The hydrogenolysis of alkanes is an important unit operation in refineries for reducing the chain length of acyclic alkanes. It also serves as a model for the hydrogenolysis of C-O and C-N bonds in various applications relevant for oil refining

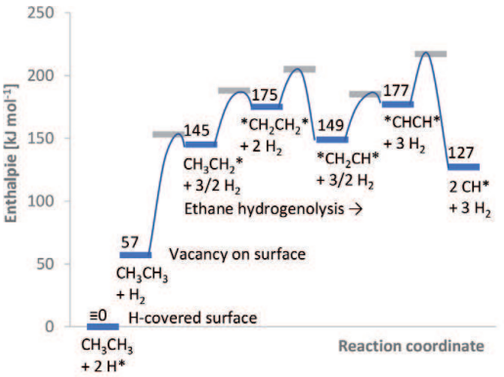

8	9	10	11
		Ni CH_2CH * +39	**Cu** CH_3CH_2 * -72
Ru $*CH_2CH$ * +51	**Rh** $*C_HC*$ +69	**Pd** CH_3CH * +12	**Ag** CH_3CH_2 * -221
Os $*CH_2CH$ * +67	**Ir** $*CH_2CH$ * +88	**Pt** CH_3C* +34	**Au** CH_3CH_2 * -133

Figure 4.
*Calculated reaction enthalpies for the elementary steps in the hydrogenolysis of ethane on a Ru(001) surface (593 K, left) and intermediates with the lowest activation free-energy barrier relative to *CH-CH* bond activation (right) [49]. Energies are relative to a surface covered with chemisorbed hydrogen (H*); * denotes coordination to the ruthenium surface.*

and biofuel generation. Cleavage of the C-C bond is preceded by a series of quasi-equilibrated dehydrogenation steps (see **Figure 4** for ethane hydrogenolysis [49]). Desorption of two chemisorbed hydrogen atoms generates the necessary adsorption sites on the surface. Physisorbed ethane dissociates stepwise via CH_3CH_2*, $*CH_2CH_2$*, $*CH_2CH$* to form *CHCH*. Activation of the C-C bond in *CH-CH* has a lower intrinsic barrier in further dehydrogenation. Cleavage of the C-C bond in the *CH-CH* surface intermediate is thought to be the rate limiting step. During the entire process, the surface is covered to a large extent with chemisorbed hydrogen (H*). The high hydrogen coverage also enhances the re-hydrogenation of the unsaturated fragments to produce methane that is desorbed from the surface.

Similar to Ru, C-C bond cleavage in more deeply dehydrogenation intermediates is preferred for Os, Rh, Ir, and Pt relative to cleavage of the C-C bond in more saturated intermediates (**Figure 4**, right). Cleavage of the C-C bond in more saturated intermediates starts to compete as one moves more to the right of the periodic table. For the group 10 metals (Ni, Pd, Pt), the most favourable mechanism is C-C activation in *CHCH*, while other intermediates have activation energies of about 40 kJ mol^{-1} suggesting that multiple routes may coexist. For the coinage metals (Cu, Ag, Au), there is a preference for cleavage of the C-C bond in the most saturated intermediate CH_3CH_2*. The overall free-energy barrier for C-C bond activation is lowest for Ru providing the highest turnover rate for *CHCH* bond cleavage. Thus, the less noble metal Ru is more active than the more noble metals. This is also consistent with experimental data that show a decrease in the turnover rate in the sequence Ru > Rh > Ir > Pt [49].

5.4 Catalysis with molecular ruthenium catalysts

Some very active molecular ruthenium (pre)catalysts were developed for catalytic hydrogenation and transfer hydrogenation. Selected examples are shown in **Figure 5**. Ruthenium hydride complexes [50] with phosphine or diamine ligands are active for the hydrogenation of many substrates. Transfer hydrogenation with ruthenium catalysts is frequently used for the reduction of ketones to alcohols [51] and amides, imines and nitriles to amines [52, 53]. Isopropanol is commonly employed as hydrogen donor [54]. The hydrogenation and transfer hydrogenation can be stereoselective if the starting material is prochiral and a chiral complex is employed [52, 55]. However, chiral BINAP catalysts can reduce only functionalised ketones in a stereoselective manner. Whereas Noyori precatalysts of the type [$RuCl_2$(diphosphane)(diamine)] enable the asymmetric hydrogenation of ß-keto esters as well as the

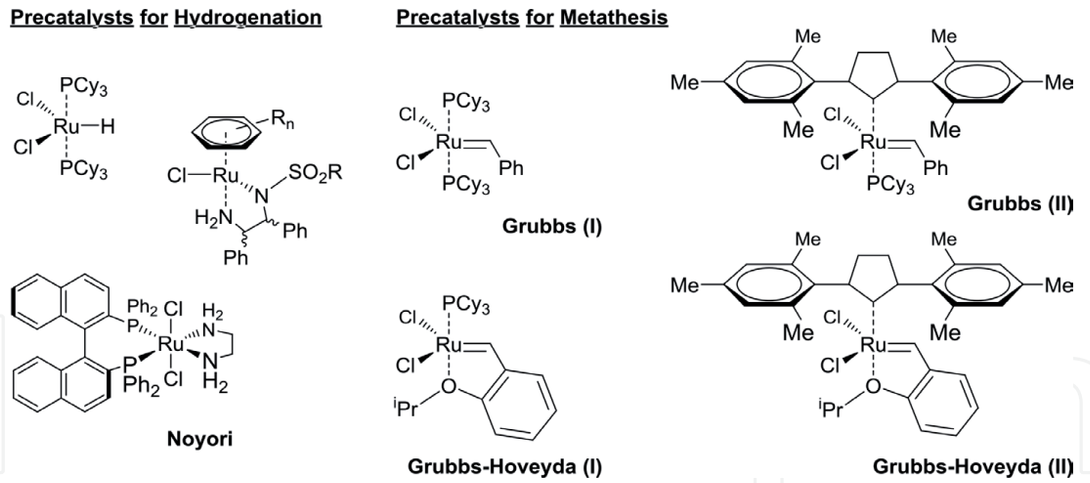

Figure 5.
Examples of molecular ruthenium complexes that are used in homogeneously catalysed hydrogenation and metathesis reactions.

reduction of prochiral ketones and aldehydes, olefins are usually not converted. The stereoselectivity is enhanced, when the substituents on the ligands differ in size. The concept of bifunctional asymmetric catalysis with ruthenium complexes has later been transferred to a variety of C-C, C-O and C-N forming reactions [56].

Ruthenium is also the central metal in the Grubbs catalysts [57], which are among the most important precatalysts for olefin metathesis. There are two generations of Grubbs catalysts (**Figure 5**). The first generation is often employed for ring-opening polymerisation (ROMP [21]) and for the synthesis of large rings by metathesis. The second generation [58] has a much higher activity. In Grubbs-Hoveyda catalysts, one of the tricyclohexylphosphine (PCy_3) ligands of the Grubbs catalysts is replaced by an aromatic ether that links to the carbon substituent. There is a wide field for ruthenium-catalysed cyclisation reactions [59]. Ruthenium *N*-heterocyclic carbene (NHC) complexes based on the second-generation Grubbs catalysts have also been applied in a variety of related transformations, such as hydrogenation [60], hydrosilylation, and isomerization [61]. Metathesis can also be combined with a second chemical transformation to tandem reaction sequences [61]. Likewise, living free radical polymerizations are feasible with ruthenium complexes [62]. An example is the polymerisation of methyl methacrylate with $[RuCl_2(PPh_3)_3]$ as a catalyst [63, 64].

6. Hydrogen adsorption on metallic ruthenium

As for the other platinum group elements, metallic ruthenium is characterised by excellent catalytic results for a variety of transformations. The interaction of molecular hydrogen with the surface of ruthenium is particularly interesting as far as catalytic hydrogenation or hydrogenolysis reactions are concerned; it will be analysed in further detail here. Accordingly, the fundamental concepts discussed here likewise are valid for transfer hydrogenation reactions.

Dissociative chemisorption of hydrogen on the surface is a pivotal step of the transformation and is often rate-limiting. The adsorption of hydrogen may be considered as competing molecular and dissociative adsorption of hydrogen (**Figure 6**) [65]. Molecular adsorption is governed by the van der Waals interactions between molecular dihydrogen and the ruthenium surface [66]. On a Ru(0001) surface with point group symmetry C_{3v} [67], the four high-symmetry adsorption sites involve binding of the hydrogen molecule to a single ruthenium atom (*on top*), a position bridging two ruthenium atoms (*brg*) or three-fold coordination at *fcc* or *hcp* sites (**Figure 6**) [67, 68].

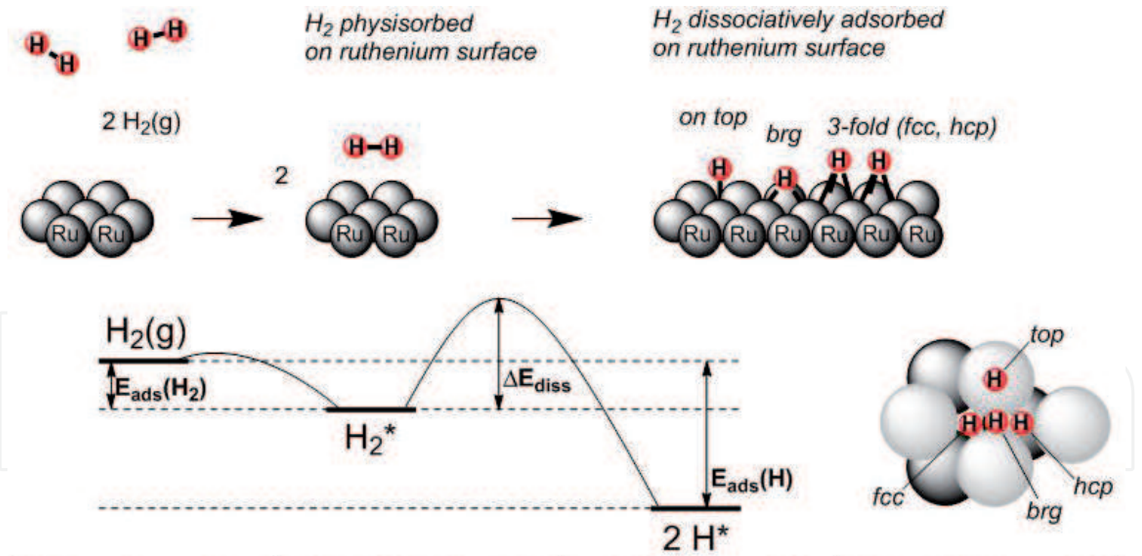

Adsorption site	$\Delta H_{ads}(H_2)$ [kJ·mol^{-1}]	ΔE_{diss} [kJ·mol^{-1}]	$\Delta H_{ads}(H)$ [kJ·mol^{-1}]
on top	-20.3	16.4	-207.9
brg	-4.8	28.9	-242.7
fcc	-4.8	41.5	-258.6
hcp	-4.8	48.2	-258.2

Figure 6.
Physisorption and chemisorption of molecular hydrogen on extended ruthenium surfaces and the C_{3v} high-symmetry adsorption sites on the Ru(0001) surface on top (u_{CM} = 0; v_{CM} = 0), brg (1/2;1/2), fcc (2/3;1/3) and hcp (1/3,2/3) (top) [67] and changes in adsorption energy for physisorption of hydrogen $E_{ads}(H_2)$, dissociation barrier ΔE_{diss} and chemisorption of hydrogen $E_{ads}(H)$ (physisorption vdW-DF2 + PBE level, [66], chemisorption GGA with periodic plane-wave basis set, 1 monolayer coverage, no correction for zero point energy [78].

Physisorption attracts a charge of −0.04 electrons to the hydrogen molecule [66]. This is consistent with promotion of dissociative adsorption of hydrogen in the presence of alkaline metal cations [69]. Electron transfer to the anti-binding orbitals of hydrogen and upward shift of the transition metal d-band centre towards the Fermi level are likely explanations.

For coordination of hydrogen in the molecular state [70], the *on top* site provides the highest adsorption energy of −20.3 kJ·mol^{-1} and the lowest dissociation barrier of 16.4 kJ·mol^{-1} [66]. Consequently, an entrance channel barrier is missing, and this dissociation channel appears to be active even for dissociation of H_2 molecules with negligible incident energy. Nevertheless, a suitable approach of the H_2 molecules to the ruthenium surface is essential for such a low dissociation barrier. Dissociation of molecular hydrogen on ruthenium is a rather slow process [69], and equilibrium is obtained only after several hours [71]. Point-like defect structures, like Ru vacancies or Ru adatoms on the surface do not seem to provide comparably low dissociation barriers. Other defects that are present at finite temperatures on the surface include steps, kinks and adatom islands [72, 73]. Low coordinated defect sites may be the preferential sites for a direct dissociative adsorption pathway on ruthenium nanoparticles [74]. Due to the low barrier, the *on top* site is likely the most reactive site for hydrogen dissociation on extended ruthenium surfaces [67]. For supported ruthenium catalysts, a rapid H_2/D_2 isotopic equilibration reaction has been reported [69]. Even so, the isotope exchange is slowed down considerably in the presence of alkaline metal cations that prevent spillover [70, 75] of hydrogen atoms to the support.

Dissociative adsorption occurs when the bonds formed between the two hydrogen atoms and the ruthenium surface are stronger than the strength of the hydrogen–hydrogen bond (460 kJ·mol^{-1}). This is the case when the hydrogen atoms adsorb at either

the *fcc* or the *hcp* hollow site (−258.6 and − 258.2 $kJ{\cdot}mol^{-1}$, respectively). Noteworthy is the relatively small difference in energy between the *fcc* and *hcp* hollow sites. As for extended surfaces of other late transition metals, hydrogen, thus, has a pronounced preference for binding to multi-fold coordination sites [76, 77]. As far as metal clusters and nanoparticles are concerned, the number of adsorption sites can differ, whereby specific 2-, 3-, and 4-fold coordination to surface atoms has been reported [76]. The barrier for surface diffusion [70] of hydrogen is rather small and was estimated to 13–21 $kJ{\cdot}mol^{-1}$. There is a small decrease of −12.1 $kJ{\cdot}mol^{-1}$ in adsorption energy with coverage θ increasing from partial (1/3) to monolayer coverage.

At low temperature, the catalytically active ruthenium surface is normally covered to a large extent with hydrogen. The surface coverage remains incomplete under reaction conditions even at elevated pressures. Thus, at 100 bar, a coverage θ of ca. 85% was calculated at room temperature, whereby it decreased to ca. 70% at increasing temperature (500 °C) [78]. Temperature-programmed desorption of hydrogen from ruthenium catalysts shows two distinct desorption peaks as a characteristic feature [71, 74]. The peaks represent strongly and weakly chemisorbed hydrogen, consistent with distinct NMR signals at −60 and − 30 ppm [79]. The corresponding heats of adsorption were determined to be 40–70 $kJ{\cdot}mol^{-1}$ (α_H) and 10 $kJ{\cdot}mol^{-1}$ (β_H), respectively, by microcalorimetry [69]. This suggests that part of the hydrogen is not dissociated over real samples. Consequently, a chemisorption stoichiometry x_M exceeding unity is frequently considered (x_M = 1.4 [74]; 2 [71, 80]; 5 [79]). Although surface processes dominate, subsurface hydrogen cannot be ruled out [70, 81]. Furthermore, the support can act as a reservoir for hydrogen [69].

Under catalytic conditions, surfaces are saturated by hydrogen or one or more adsorbed intermediates. This leads to strong co-adsorbate interactions. These interactions are not accounted for in kinetic models built on Langmuir isotherms. In real catalysts, however, mostly supported metal nanoparticles are employed, where these co-adsorbate interactions are lessened. The curvature of the nanoparticles allows for adlayer relaxation [82]. Thus, CO hydrogenation rates on Ru clusters are much higher at high CO coverage than predicted based on a Langmuir approach [83]. Activation of adsorbed CO by reaction with surface hydrogen results in transition states that occupy less space than [82] the pair of surface moieties that they replace. This causes the overall activation energy to decrease with increasing CO* coverage.

Interestingly, species co-adsorbed on a ruthenium surface may show a strong tendency to segregate. Thus, with carbon monoxide and hydrogen co-adsorbed on a Ru(0001) surface, the carbon monoxide molecules form islands that are surrounded by hydrogen atoms [84]. At cryogenic temperatures, the carbon monoxide molecules form triangular islands of up to 21 molecules located on the *on top* sites. Through this type of island formation, long-range lateral CO-H repulsive interactions are minimised. With an increase in temperature, the carbon monoxide molecules shift to the *hcp* sites and the island size decreases to 3–6 molecules [84]. Through this decrease in domain size, repulsive CO–CO interactions that become more prominent upon increasing the temperature are reduced. The proximity of the carbonyl and hydride adsorbate species to one another (3.0–3.7 Å distance) [84] explains the propensity of ruthenium surfaces for Fischer-Tropsch reactions. The ensuing CO bond cleavage is facilitated by the formation of partially hydrogenated CHO and COH intermediates.

7. Supports for heterogeneous ruthenium catalysts

For applicable heterogeneous catalysts, metallic ruthenium is supported in form of ruthenium nanoparticles on a suitable support. This ensures a high dispersion and a large surface area of ruthenium. Carbon supports, in particular active carbons

and carbon nanotubes, and oxidic supports are frequently employed. To ensure that the ruthenium nanoparticles are immobile on the support surface under the catalytic conditions, there has to be a sufficiently strong interaction between metal nanoparticles and the support. Otherwise, there would be pronounced sintering of the ruthenium nanoparticles that would lead to gradual loss of the catalytic activity. The support also influences the electron density in the ruthenium nanoparticles, thereby lowering or increasing the Fermi level. For oxidic supports, the interaction between nanoparticles and the support cannot be too strongly pronounced, because ruthenium cations tend to diffuse into the bulk of the support material.

For carbonaceous materials anchoring sites have to be generated on the surface to anchor the ruthenium nanoparticles. Providing high surface area, active carbons and carbon nanotubes thus usually undergo an oxidative pre-treatment. As a result, oxygenated moieties are generated to which the ruthenium nanoparticles strongly bind. In this aspect, the property of ruthenium being at the borderline between noble and non-noble metals is exploited. Under more driving reductive conditions of a hydrogen atmosphere, however, the susceptibility of carbon carriers to methanation is challenging for carbon-supported ruthenium catalysts, because it leads to degradation of the carrier and sintering of the ruthenium clusters. Compared to active carbons, carbon nanotubes lend a more defined support and higher stability.

Carbon nanotubes combine physicochemical properties that make them interesting as support for ruthenium, such as high surface area, good mechanical strength, chemical and thermal stability, high heat and electric conductivity. So far, the high costs incurred by elaborate synthesis procedures [85–89] hinder their more widespread use as well-defined catalyst supports [90]. For immobilisation of metal nanoparticles, anchoring sites need to be generated on the surface of the carbon support. A method of preparing a Ru/CNT catalyst with supported ruthenium nanoparticles involves treatment of the CNT in refluxing nitric acid [91]. Deposition-precipitation of the ruthenium precursor $Ru(NO)(NO_3)_x(OH)_y$ followed by reduction of the precursor to the metal with molecular hydrogen provides well-dispersed surface-anchored Ru nanoparticles (**Figure 7**) [29]. Such catalysts are excellent hydrogenation and hydrogenolysis catalysts (see below).

Oxidic supports that are frequently employed comprise silica, alumina (mostly γ-Al_2O_3), zirconia, ceria and the corresponding mixed oxides. Even though amorphous materials provide the necessary high surface area, they often are associated with certain distribution of surface functions. Yet as surface groups, they may be harmful in catalysis. The presence of different surface sites often leads to alternative

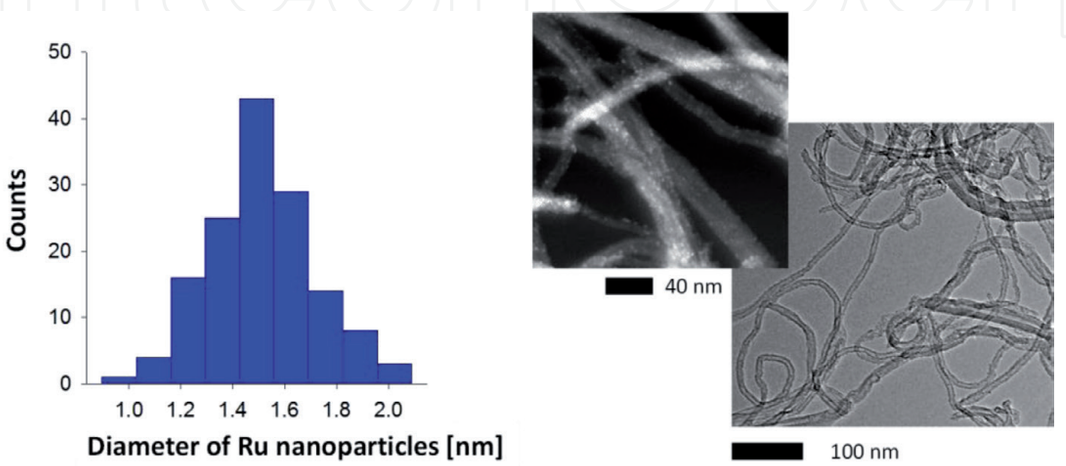

Figure 7.
Particle size distribution of the ruthenium nanoparticles for a typical Ru/CNT catalyst and representative transmission electron microscopy images [29]. The carbon nanotubes are Baytubes C 150 P.

Activated carbons		*Oxidic supports*		
Adsorbent	**Hydrophobicity index (HI)**	**Adsorbent**	**Pore size [Å]**	**Hydrophobicity index (HI)**
Darco-KBB	26.3	Y	7.35	0
SX1G	26.2	Beta	5.95	1.4
F300	160	ZSM-5, Silicalite-1	4.46	8, 15.2
Duksan	296	MCM-41	16–42	9

Table 1.
Comparison of the hydrophobicity of carbon supports (left) and oxidic supports (right) [27]; the pore size of zeolites (Beta, Y, ZSM-5, Silicalite-1 [92]) and mesoporous materials (MCM-41 [93]) is the maximum diameter of a sphere that can diffuse through the channels.

catalytic pathways that result in reduced selectivity of the transformation. Instead, more defined support materials are nanoporous zeolites, such as zeolite Y, Beta, and ZSM-5, or mesoporous materials, such as MCM-41. The internal pore system (**Table 1**) provides a uniform environment for the catalytic transformation. Nevertheless, many biomolecules are too large to enter the pore system and need to be cut to molecular entities first. Catalysis at the pore mouth or using molecular catalysts is an option for the depolymerisation step.

The hydrophobicity index (HI) is a good measure for assessing the internal hydrophobicity of porous materials. HI can be determined by the competitive adsorption of a toluene-water mixture. The hydrophobicity index is defined by the ratio of the adsorption capacity for toluene ($Q_{Toluene}$) to that of water (Q_{Water}). For comparison, the reported HIs of some activated carbons, microporous zeolites, and mesoporous materials are listed in **Table 1** [27]. The hydrophobicity index (HI) of typical zeolites, such as beta, Y and ZSM-5 is low (HI = 1.4, 0, 8, respectively), which is consistent with the hydrophilic nature of the pore walls. This is attributed to a certain polarity of the zeolite walls that results from the aluminium atoms substituting a certain part of the silicon atoms. All-silica zeolites, such as Silicalite-1, are clearly more hydrophobic (HI = 15.2) and more resemble activated carbons which are commonly regarded as hydrophobic adsorbents.

Unsupported metal nanoparticles can be employed as quasi-homogeneous catalysts but need to be stabilised by ligation or generation of an electric double layer to prevent agglomeration of the nanoparticles [94]. Upon decreasing the size of the metal nanoparticles, the boundary of the metallic state is obtained for two-shell clusters of about 1.5 nm in diameter [95]. Ruthenium nanoparticles stabilised with a thin layer of ionic liquid tartaric acid tetraoctylammonium $[TA^{2-}][N^{+}_{8888}]_2$ or glycine tetraoctylammonium $[Gly^{-}][N^{+}_{8888}]$ have shown excellent catalytic properties for the hydrogenation of challenging substrates. One example is the conversion of nitrobenzene to cyclohexylamine. Catalytic activity and selectivity of the quasi-homogeneous nanoparticle catalyst resemble that of a corresponding supported Ru/C catalyst. Upon switching to the less polar ionic liquid dimethylglycine tetraoctylammonium $[Me_2Gly^{-}][N^{+}_{8888}]$, the selectivity changes to the reaction intermediate aniline. This is attributed to the relative binding strength of ionic liquid and intermediates to the ruthenium surface. Thus, the use of ionic liquids as stabiliser lends a ready method to tailor the properties of the catalyst. Interestingly, ionic liquid-stabilised nanoparticles are readily supported on a mesoporous support [96, 97] thus turning the quasi-homogeneous catalyst into a true heterogeneous catalyst. Noteworthy, the catalytically active site remains in the flexible environment of the ionic liquid [98] which imparts beneficial properties to the catalyst [99]. During the chemical transformation,

the active species can easily adapt to the geometry changes that occur during the path from reactant to transition and product state. Moreover, the equivalence of all catalytically active sites is readily maintained which can render enhanced selectivity. The ionic liquid then again provides a polar medium for tailoring the adsorption of the substrate molecules and desorption of the product molecules [100] that precede and succeed the catalytic reaction, respectively. Interestingly, in supported films of ionic liquid. Rates as well as chiral induction can be enhanced, as was demonstrated for the hydrogenation of the prochiral substrate acetophenone over [Ru((R)-BINAP)$(PPh_3)_nCl_{3-n}$], n = 0, 1 [101]. A useful feature of such supported catalysts is that fixed-bed reactor technology common in continuous chemical processes can be employed [97].

8. Biomass conversion with ruthenium catalysts

About 1% of the incoming solar radiation on earth is captured for generating biomass [102]. This energy is utilised in photosynthesis [103] to build a myriad of complex molecules [104] such as carbohydrates, lignin, proteins, fats and oils, and terpenes. In this way about 170 x 10^9 t/a of complex substances are produced annually [105]. In plants, the radiation use efficiency is controlled by the net-photosynthetic capacity and the canopy structure [106, 107]. Cultivars with a heavy canopy and long growth period are able to harness more solar radiation [108]. A large fraction of the produced biomass is characterised by a high oxygen content (**Table 2**). Cellulose, a polymeric carbohydrate, and lignin a randomly linked phenolic polymer constitute a major fraction of plant biomass (around 95% [109]). Their oxygen content is much higher than that of fossil resources such as crude oil, natural gas and coal (**Table 2**). About 56% of the oil extracted from the resources is utilised to make liquid fuels (70.6%) for transport purposes [2]. About 14% of the oil and 8% of the gas extracted from these resources is utilised to make petrochemicals. Both fuels and many petrochemical products are characterised by a low oxygen-to-carbon ratio. Some examples are given in **Table 2**. Consequently, in order to exploit biomass, a controlled de-functionalisation is necessary. In particular, efficient strategies are needed to decrease the oxygen-to-carbon ratio.

At present, biorefinery routes [118, 119] have been improved to more efficiently exploit biomass feedstock. In the production of bioethanol from lignocellulosic biomass, e.g., by hydrolysis of wood with dilute acids, hexoses are obtained that are good feedstock for fermentation [4]. The target product then needs to be separated from the aqueous fermentation broth. By producing ethanol in this way, about 8.7% of the mass and 11% of the energy contained originally in the wood are found in the product [109]. The remainder are 37% by-products and 40% waste products, mostly carbon dioxide (36%) that need to be utilised or disposed. Green chemistry metrics [120], notably the E-factor and atom economy, clearly need to be improved further. One option is the direct chemical conversion of lignocellulosic biomass in a single reaction step over a multifunctional catalyst as outlined below. Such transformation follows the principles of a molecular assembly line. Thus, efficient and frequently multistep catalysis is one of the keys for realising fast and highly selective conversion of biomass [109]. Before the particular aspects of ruthenium catalysts in biomass conversion are considered, the general architecture and the availability of biomass is analysed briefly. Lignocellulose makes up the structural components of plants and a large fraction of the plant biomass available for producing platform chemicals. Wood, e.g., is essentially composed of cellulose (39–45%), hemicelluloses (27–32%) and lignin (22–31%) [121].

	Category	Compound		O/C
Natural compound	Sugar-based	Cellulose $(C_6H_{10}O_5)_n$		0.83
		Carbohydrates $C_6H_{10}O_5$ [*7]		0.83
		Glucose $C_6H_{10}O_6$		1
	Lignin-based	Lignocellulose [*6]		0.8–0.9
		Lignin [*1]		0.3–0.4
	Other	Proteins $C_{147}H_{228}O_{46}N_{40}S$ [*7]		0.31
		Lipids $C_{53}H_{89}O_6$ [*7]		0.11
Derived product	Fuels	Ethanol		0.5
		Biodiesel [*4]		0.15
Fossil feedstock	Coal	Peat [*5,8]	Increasing degree of coalification [*2]	0.37–0.66
		Lignite [*5]		0.23
		Black [*3]		0.03–0.15
		Bituminous [*3]		0.03–0.10
		Anthracite [*3]		0.02–0.05
	Crude oil [*9]	Heavy (Venezuela) [*10]		0.02
	Natural gas	Methane		0
Derived product [*11]	Fuels	Petroleum [*3]		<0.2
		Diesel [*4]		0
	Petrochemicals	BTX		0
		Propene		0
		Ethene		0
		Polyethylene		0

*[*1] [110]; [*2] increasing degree of coalification relates with decreasing O/C ratio; [*3] originating from Pennsylvania [4]; [*4] [111]; [*5] [112]; [*6] [113]; [*7] [114]; [*8] [115]; [*9] [116]; [*10] [117]; [*11] for global mass flows refer to [5];*

Table 2.
Oxygen content of typical components of biomass in comparison to fossil resources and selected derived products.

9. Sustainable feedstock from biomass

Cellulose is an important structural component of the cell wall of green plants, many forms of algae and the oomycetes. Many bacteria secrete it to form biofilms [122]. Plants build about 10^{11}–10^{12} t/a of cellulose annually mostly in combination with hemicelluloses and lignin [123]. This makes cellulose the most abundant organic polymer on Earth [124]. Cellulose is a polysaccharide, a linear chain with the formula $(C_6H_{10}O_5)_n$ consisting of 7,000–15,000 of $\beta(1 \rightarrow 4)$ linked D-glucose units [125].

Even though hemicellulose is a polysaccharide often associated with cellulose, cellulose and hemicellulose have distinct compositions and structures. Hemicellulose is a branched polymer but cellulose is unbranched. Whereas hemicellulose is built from diverse sugars, cellulose is derived exclusively from glucose. For instance [126], besides glucose, sugar monomers in hemicelluloses can include hexose sugars, such as mannose and galactose, and pentose sugars, such as xylose and arabinose. Unlike cellulose, the side chains in hemicelluloses are often modified with acetyl and glycosyl groups.

Lignin is a randomly linked polymer (**Figure 8**) comprising phenolic *p*-hydroxyphenyl (**H**), guaiacyl (**G**) and syringyl (**S**) moieties (see also **Figure 9**) that are linked *via* ether linkages (*ß-O-4'*, *α-O-4'*, *4-O-5'*), biphenyl (*5–5'*), resinol *(ß-ß')*, and other condensed linkages (*ß-5′*, *ß-1′*) as well as dibenzodioxocin, and phenylcoumaran linkages [109, 127]. The complex structure of lignin is the result of the biosynthetic pathway that involves oxidation of phenolic precursors to radicals followed by radical coupling that leads to stepwise build-up of the lignin structure [128].

The components of plant biomass are normally fractionated using biochemical [129, 130], thermochemical [131] and/or catalytic methods [132]. Lignin is particular is that respect that it is highly resistant to depolymerisation. Consequently, at present the lignin fraction is often used to a large extent as fuel for heat generation. Methods have been developed to utilise the phenolic structure for producing polymers, resins, additives, fuels and chemicals. Common methods for depolymerisation of lignin into monomeric phenolic compounds involve pyrolysis [133–136], enzyme [137, 138], acid or base [139, 140] catalysed hydrolysis, and hydrogenolysis [141–143]. Catalysts based on metallic ruthenium are frequently employed in hydrolysis and hydrogenolysis of the ether linkages or hydrodeoxygenation [110, 144] of the phenol products (*vide supra*).

In subsequent downstream processing, the biomass fractions are converted to platform chemicals. Based on the generally accessible biomass, platform molecules (**Figure 9** [4]) include organic acids, such as propionic acid, 3-hydroxypropionic acid, succinic acid, fumaric acid, itaconic acid, and levulinic acid [145], fat and oil-derived polyols, in particular glycerol, as well as sugar-derived polyols such as sorbitol and xylitol. Additional platform chemicals are alcohols such as methanol, ethanol, and propanol, cyclic ethers, such as furfural and 5-hydroxymethylfurfural, and terpenes, such as isoprene. Such platform molecules can be exploited as fuels

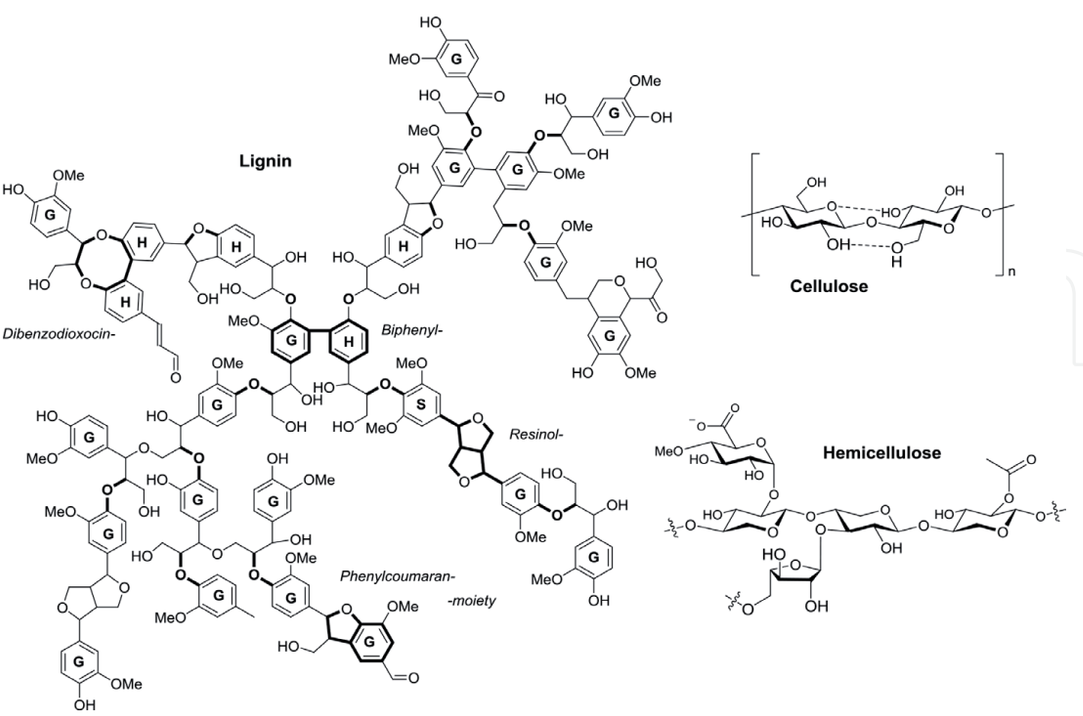

Figure 8.
*Chemical structure of important biomass fractions, lignin (left), cellulose with 1,4-glycosidic linkages and selected hydrogen bonds (right, top) and the common molecular motif of hemicellulose (right, bottom). For the structure of lignin, the characteristic aromatic p-hydroxyphenyl (***H***), guaiacyl (***G***) and syringyl (***S***) moieties as well as aromatic ether linkages (-**O**-), dibenzodioxocin, biphenyl, resinol, and phenylcoumaran linkages [109, 127] were marked.*

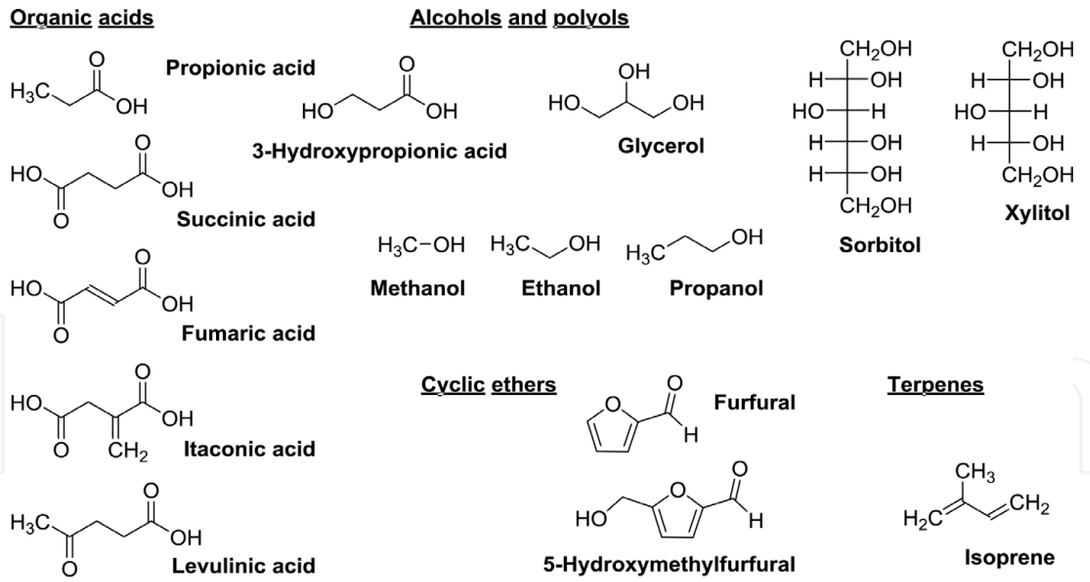

Figure 9.
Biomass derived platform chemicals.

and industrially relevant chemicals or are readily transformed into such fuels and chemicals. Ruthenium-based catalysts are frequently employed in key transformations such as hydrogenation, hydrogenolysis, and oxydehydrogenation [146]. Compared to nickel-based catalysts, ruthenium-based catalysts provide higher activity and better stability that result in lower catalyst loadings, longer lifetimes and less pronounced deactivation. Although ruthenium-based catalysts are more expensive, these costs are offset by their higher activity and their lower tendency to leach.

10. Ruthenium catalysts in cellulose conversion

While first-generation bioethanol is produced on the million t/a scale, production of second-generation bioethanol from cellulosic biomass is still in its infancy [4]. The challenge is the enzyme- or acid-catalysed hydrolysis of lignocellulosic materials to simple sugars that can be fed into fermentation, from which ethanol is separated by distillation [147]. A one-step catalytic conversion of cellulosic biomass (bagasse and corn stalk) to bioethanol has been realised with a ruthenium-based catalyst [148]. The catalyst comprises well-dispersed Ru and WO_x nanoparticles on a H-ZSM-5 solid acid support. Under catalytic conditions, also highly dispersed Ru_3W_{17} alloy nanoparticles are formed. In a cascade reaction cellulose undergoes hydrolysis on moderately acidic sites of the H-ZSM-5 support, followed by glucose retro-aldol condensation to glycolaldehyde over WO_x and hydrogenation over Ru to yield ethylene glycol that is dehydrated and finally hydrogenated to ethanol on the Ru_3W_{17} alloy sites.

Interestingly, subcritical water is an efficient reaction medium for cellulose conversion [149, 150]. Thus, cellulose is converted to polyols over ruthenium supported on crosslinked polystyrene [149, 151]. Swelling of the polymer [152] thereby facilitates access of the substrate to the catalytic sites.

A carbon-supported ruthenium hybrid catalyst with a specific surface area of 1200 $m^2\ g^{-1}$ was employed for the direct hydrogenolytic cleavage of cellulose to sorbitol [153]. High microporosity and low acidity of the carbon support favour high dispersion of the metallic ruthenium. Interestingly, ball-milling of cellulose with carbon supported ruthenium provides enhanced conversions and selectivities to sorbitol [154, 155].

Selective conversion of cellulose to sorbitol is achieved *i.a.* by use of bi-functional ruthenium catalysts supported on sulphated zirconia and sulphated silica-zirconia [156]. Tetragonal zirconia, associated with generation of superacidity, is the active phase for cellulose depolymerisation that accompanies the hydrogenation function of ruthenium. Also, zeolite- [146, 157] and silica- [158] supported ruthenium nanoparticles are suitable for the hydrogenation of glucose to the sugar alcohol sorbitol.

Hydrogenolysis of sorbitol to ethylene glycol and 1,2-propanediol is obtained over bifunctional Ru-WO_x/CNT catalysts [159]. Furthermore, addition of $Ca(OH)_2$ proved beneficial for the hydrogenolysis activity.

11. Ruthenium catalysts in lignin conversion

Hydrogenolysis of lignin involves reductive bond cleavage of C-O bonds linking the phenolic moieties, thereby generating hydrogenated and therefore less reactive monomeric species. For the reduction step, ruthenium catalysts are frequently employed. A variety of reducing agents have been suggested [141, 160, 161], such as hydrogen [142], carbon monoxide, formic acid ($HCOOH/NEt_3$ [53]), methanol, ethanol, isopropyl alcohol [54], acetonitrile, acetone. The energy needed for producing the reductant and the associated CO_2-footprint ought to be taken into account when the lignin-derived products are utilised as biofuels [162]. Supercritical fluids as solvent have been claimed to produce fewer solid residues and provide higher biomass conversions [163, 164]. Catalytic transfer hydrogenolysis of corn stover lignin in supercritical ethanol with a Ru/C catalyst yields bio-oil with a high fraction of monomeric moieties [163]. The key transformation is the reductive cleavage of ether linkages. Sequential extraction with a series of solvents differing in polarity results in monomer fractions that are enriched in alkylated phenols, guaiacols, syringols and hydrogenated hydroxycinnamic acid derivatives (**Figure 10**).

For using bio-oils as fuel, hydrotreating is necessary for lowering the oxygen content. Hydrotreating increases stability and energy density while decreasing the viscosity of the bio-oils. Ruthenium catalysts are often used in this hydrogenolytic upgrading of bio-oils. Even though zeolites are a good support material, substituted phenols cannot enter the micropores of typical zeolites. One concept for overcoming this challenge are catalysts comprising hierarchical pore systems. Thus, Ru supported on mesoporous ZSM-5 with a characteristic pore size of 4.5–4.7 Å of the MFI lattice channels (**Figure 11**) [92] and the mesopore system aligned to the *b*-axis was found to be effective for the hydrodeoxygenation of phenolic biomolecules [144]. For comparison, the Van-der-Waals radius of the syringol molecule is estimated to

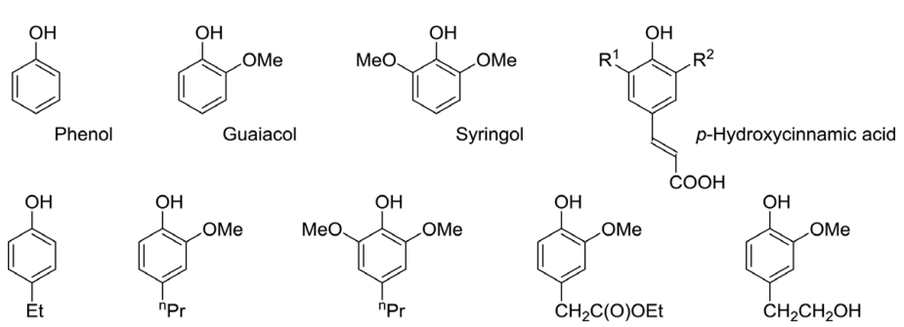

Figure 10.
Phenol-, guaiacol-, syringol- and hydroxycinnamic acid (top row)-derived monomers typically found in lignin hydrogenolysates (bottom row).

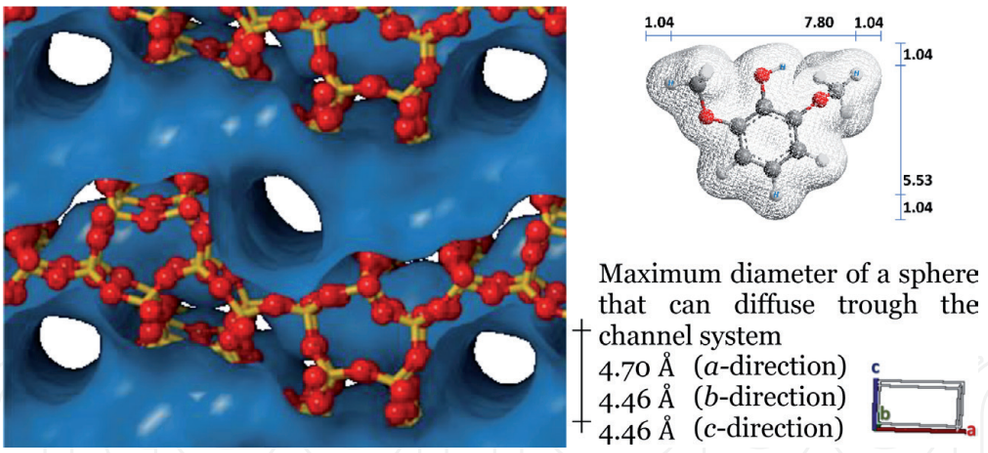

Figure 11.
Comparison of the characteristic dimensions of syringol (top right) and the three-dimensional MFI pore system of zeolite ZSM-5, here viewed down the b-direction (left; not to scale; red, oxygen atoms; orange, silicon atoms), and maximum diameter of a sphere that can diffuse through the channel system (bottom right).

be 9.88 × 7.61 Å (**Figure 11**) based on the distance of the outermost hydrogen atoms [165] and a Van-der-Waals radius for hydrogen of 1.04 Å [166]. Only at the channel entries do the open mesopores expose acid sites to the approach of bulky molecules necessary for catalysing the cleavage of the phenolic C-O bonds. This type of catalyst was found to effectively catalyse the hydrodeoxygenation of phenol and 2,6-dimethoxyphenol at 4.0 MPa H_2-pressure and a temperature of 150 °C [144]. Conversions were > 99.5 and 97.5% after a 4 h reaction time, respectively; product selectivities to cyclohexane were accordingly 95.0 and 70.0%.

12. Conclusions on biomass transformation with ruthenium catalysts

Ruthenium, a late transition element, provides catalytic pathways that make it highly promising for catalysts applied for biomass conversion. Biomass, a globally available resource, is a sustainable feedstock for producing platform chemicals, that could substitute the current fossil-based platform chemicals in the chemical industry. However, in order to implement further processes in small and large-scale biorefineries, more efficient transformations will be required. Here, the distinct catalytic functions provided by ruthenium and ruthenium complexes could open new pathways. Biomass largely consists of complex molecules that comprise oxygen and other heteroatoms. Catalytic transformations need to accommodate for these heteroatoms, because molecules with heteroatoms tend to adsorb strongly to catalytic sites possibly causing substrate- or product inhibition. However, the preferential adsorption of chemical moieties associated with heteroatoms on the catalytically active site can be exploited for directing catalytic transformations. The principle has been explored for the consecutive hydrogenation of unsaturated moieties on a molecular assemble line. In this context, it is useful considering the concept of orthogonal catalytic functions, where a catalyst preferentially binds and transforms a selected chemical entity without hindering other catalysts that may be added for realising preceding or subsequent catalytic transformations.

In this context, the catalytically highly active element ruthenium embodies unique features. Ruthenium does not form binary hydrides that are stable under usual catalytic conditions. Nevertheless, metallic ruthenium can dissociate molecular hydrogen. Under an atmosphere of hydrogen, the surface of metallic ruthenium is covered with hydrogen atoms. Adsorption states and chemical reactivity of this hydrogen is well understood. Desorption of a fraction of the

hydrogen provides the empty coordination sites necessary for co-adsorption of reactant molecules. Typically following a Langmuir-Hinshelwood-type mechanism, hydrogen atoms can be transferred to unsaturated moieties. Remarkably, ruthenium can also form and cleave C-C, C-O and C-N bonds. Combined with its strong propensity for hydrogenation, this ability gives rise to hydrogenation, hydrogenolysis and hydrodeoxygenation transformations that make ruthenium catalysts so interesting for biomass conversion. Noteworthy are the distinct catalytic transformations that can be realised with ruthenium catalysts. Selected examples for intriguing transformations of biomolecules and bio-derived molecules have been discussed above.

Understanding the interaction of adsorbed molecules with ruthenium surfaces, the nature of adsorption states, binding energies and structures of the adsorption complexes lies at the heart of rational design of catalysts that are specific for the conversion of the chosen chemical entity in biomass. It is anticipated that new transformations will be realised based on the unique catalytic functions provided by heterogeneous and homogeneous ruthenium catalysts. Serving as important tools for the synthetic chemist, these transformations will bolster the use of biomass as sustainable feedstock for the chemical industry.

Acknowledgements

With financial support from the state government of North Rhine-Westphalia and the Indo-German Science & Technology Centre (IGSTC). TEM acknowledges the support of Fraunhofer-Institut für Umwelt-, Sicherheits- und Energietechnik UMSICHT. P. Tomkins and E. Gebauer-Henke are gratefully acknowledged for the characterisation of the Ru/CNT catalyst, C. Herwartz (GFE) for TEM measurements, M. Hermesmann for the literature searches on environmental impact, as well as D. Panke for drawing the chemical structure of biomass fractions.

Conflict of interest

There are no conflicts of interest to declare.

Notes

For compiling **Figure 2**, image 1961095 was obtained with the standard licence from Shutterstock.

Abbreviations and nomenclature

*	Surface adsorbed species
Θ	Coverage
x_M	Chemisorption stoichiometry
ads	Adsorption
AN	Aniline
CA	Cyclohexylamine
CNT	Carbon nanotube
diss	Dissociation
GFE	Gemeinschaftszentrum für Elektronenmikroskopie

HI	Hydrophobicity index
M	Metal
NB	Nitrobenzene
NMR	Nuclear magnetic resonance
ROMP	Ring opening metathesis polymerisation
Beta	Zeolite Beta with BEA structure
H-ZSM-5	Zeolite ZSM-5 with MFI structure in the proton form
MCM-41	Mesoporous material
Y	Zeolite Y with FAU structure
brg	bridging adsorption site
fcc	three-fold coordination
hcp	three-fold coordination
on top	terminal adsorption site
a	annum
kJ	kilojoule
t	metric ton
TW	Terawatts

IntechOpen

Author details

Thomas Ernst Müller
Carbon Sources and Conversion, Ruhr-Universität Bochum, Bochum, Germany

*Address all correspondence to: thomas.mueller@ls-csc.ruhr-uni-bochum.de

IntechOpen

© 2021 The Author(s). Licensee IntechOpen. This chapter is distributed under the terms of the Creative Commons Attribution License (http://creativecommons.org/licenses/by/3.0), which permits unrestricted use, distribution, and reproduction in any medium, provided the original work is properly cited. CC BY

References

[1] Tomkins P, Müller TE. Evaluating the carbon inventory, carbon fluxes and carbon cycles for a long-term sustainable world. Green Chemistry. 2019;21(15):3994-4013.

[2] The Future of Petrochemicals. IEA International Energy Agency; 2018.

[3] Jacobson MZ, Delucchi MA. Providing all global energy with wind, water, and solar power, Part I: Technologies, energy resources, quantities and areas of infrastructure, and materials. Energy Policy. 2011;39(3):1154-69.

[4] Mika LT, Cséfalvay E, Németh Á. Catalytic Conversion of Carbohydrates to Initial Platform Chemicals: Chemistry and Sustainability. Chemical Reviews. 2018;118(2):505-613.

[5] Levi PG, Cullen JM. Mapping Global Flows of Chemicals: From Fossil Fuel Feedstocks to Chemical Products. Environmental Science & Technology. 2018;52(4):1725-34.

[6] Puchtel IS. Platinum Group Elements. In: White WM, editor. Encyclopedia of Geochemistry. Switzerland: Springer International Publishing; 2016.

[7] Zientek ML, Loferski PJ. Platinum-Group Elements—So Many Excellent Properties. Reston, VA; 2014. Contract No.: 2014-3064.

[8] Crundwell FK, Moats MS, Ramachandran V, Robinson TG, Davenport WG. Platinum-Group Element. Extractive Metallurgy of Nickel, Cobalt and Platinum Group Metals. Surface Coating and Modification of Metallic Biomaterials. 2011. p. 1-18.

[9] Ruthenium [Internet]. Thieme Gruppe. 2006 [cited 2006/12/17]. Available from: https://roempp.thieme.de/lexicon/RD-18-02130.

[10] Yuan H, Laughlin DE, Zhu X, Lu B. Ru+oxide interlayer for perpendicular magnetic recording media. Journal of Applied Physics. 2008;103(7):07F513.

[11] Wulfsberg G. Hydrides, Alkyls, and Aryls of the Elements. Inorganic Chemistry. Sausalito, CA, US: University Science Books; 2000. p. 978.

[12] Bouten PCP, Miedema AR. On the heats of formation of the binary hydrides of transition metals. Journal of the Less Common Metals. 1980;71(1):147-60.

[13] Binns J, He Y, Donnelly M-E, Peña-Alvarez M, Wang M, Kim DY, et al. Complex Hydrogen Substructure in Semimetallic RuH4. The Journal of Physical Chemistry Letters. 2020;11(9):3390-5.

[14] Morris RH. Estimating the Wavenumber of Terminal Metal-Hydride Stretching Vibrations of Octahedral d6 Transition Metal Complexes. Inorganic Chemistry. 2018;57(21):13809-21.

[15] Soini TM, Genest A, Nikodem A, Rösch N. Hybrid Density Functionals for Clusters of Late Transition Metals: Assessing Energetic and Structural Properties. Journal of Chemical Theory and Computation. 2014;10(10):4408-16.

[16] Müller TE, Ingold F, Menzer S, Mingos DMP, Williams DJ. Platinum (I) dimers and platinum (0) triangles with polyaromatic phosphine ligands. Journal of organometallic chemistry. 1997;528(1-2):163-78.

[17] Meng X, Wang F, Jin G-X. Construction of M–M bonds in late transition metal complexes. Coordination Chemistry Reviews. 2010;254(11):1260-72.

[18] Mingos DMP. High nuclearity clusters of the transition metals and a re-evaluation of the cluster surface analogy. Journal of Cluster Science. 1992;3(4):397-409.

[19] Luh T-Y, Lin W-Y, Lai G. Determination of the Orientation of Pendants on Rigid-Rod Polymers. Chemistry – An Asian Journal. 2020;15(12):1808-18.

[20] Dragutan I, Dragutan V. Ruthenium allenylidene complexes. A promising alternative in metathesis catalysis. Platinum Metals Review. 2006;50(2):81-94.

[21] Muhlebach A, Van Der Schaaf PA, Hafner A, Kolly R, Rime F, Kimer HJ. Ruthenium catalysts for ring-opening metathesis polymerization (ROMP) and related chemistry. NATO Science Series II: Mathematics, Physics and Chemistry. 2002;56(Ring Opening Metathesis Polymerisation and Related Chemistry):23-44.

[22] Donohue PC, McCann EL, III. Novel perovskites M2IILnIIIRuVO6 as emission control catalysts. Materials Research Bulletin. 1977;12(5):519-24.

[23] Cairns JF, Hodgson DR, inventors; Imperial Chemical Industries PLC, UK . assignee. Electrode patent EP479423A1. 1992.

[24] Schmidt T, Gürtler C, Kintrup J, Müller TE, Loddenkemper T, Gerhartz F, et al., inventors; Bayer MaterialScience AG, Germany . assignee. Method for production of chlorine by gas phase oxidation on nano-structured ruthenium carrier catalysts patent WO2011012226A2. 2011.

[25] Williams RJP. Possible functions of chains of catalysts. Journal of Theoretical Biology. 1961;1(1):1-17.

[26] Heidary N, Ly KH, Kornienko N. Probing CO2 Conversion Chemistry on Nanostructured Surfaces with Operando Vibrational Spectroscopy. Nano Letters. 2019;19(8):4817-26.

[27] Xie L-H, Xu M-M, Liu X-M, Zhao M-J, Li J-R. Hydrophobic Metal–Organic Frameworks: Assessment, Construction, and Diverse Applications. Advanced Science. 2020;7(4):1901758.

[28] Kim S, Lee H-E, Suh J-M, Lim MH, Kim M. Sequential Connection of Mutually Exclusive Catalytic Reactions by a Method Controlling the Presence of an MOF Catalyst: One-Pot Oxidation of Alcohols to Carboxylic Acids. Inorganic Chemistry. 2020;59(23):17573-82.

[29] Tomkins P, Gebauer-Henke E, Müller TE. Molecular Assembly Line: Stepwise Hydrogenation of Multifunctional Substrates over Catalyst Mixtures. ChemCatChem. 2016;8(3):546-50.

[30] Saadatjou N, Jafari A, Sahebdelfar S. Ruthenium Nanocatalysts for Ammonia Synthesis: A Review. Chemical Engineering Communications. 2015;202(4):420-48.

[31] Anon. KBR's KAAP Ammonia Plant Design, Proven in Trinidad, Available for 2000 MTPD. IP.com Journal. 2012;12(5B):68.

[32] Iost KN, Borisov VA, Temerev VL, Surovikin YV, Pavluchenko PE, Trenikhin MV, et al. Study on the metal-support interaction in the Ru/C catalysts under reductive conditions. Surfaces and Interfaces. 2018;12:95-101.

[33] Morgan E, Manwell J, McGowan J. Wind-powered ammonia fuel production for remote islands: A case study. Renewable Energy. 2014;72:51-61.

[34] Valera-Medina A, Xiao H, Owen-Jones M, David WIF, Bowen PJ. Ammonia for power. Progress

in Energy and Combustion Science. 2018;69:63-102.

[35] Rouwenhorst KHR, Van der Ham AGJ, Mul G, Kersten SRA. Islanded ammonia power systems: Technology review & conceptual process design. Renewable and Sustainable Energy Reviews. 2019;114:109339.

[36] Kitano M, Inoue Y, Sasase M, Kishida K, Kobayashi Y, Nishiyama K, et al. Self-organized Ruthenium–Barium Core–Shell Nanoparticles on a Mesoporous Calcium Amide Matrix for Efficient Low-Temperature Ammonia Synthesis. Angewandte Chemie International Edition. 2018;57(10):2648-52.

[37] Ju X, Liu L, Yu P, Guo J, Zhang X, He T, et al. Mesoporous Ru/MgO prepared by a deposition-precipitation method as highly active catalyst for producing COx-free hydrogen from ammonia decomposition. Applied Catalysis B: Environmental. 2017;211:167-75.

[38] Yao L, Shi T, Li Y, Zhao J, Ji W, Au C-T. Core–shell structured nickel and ruthenium nanoparticles: Very active and stable catalysts for the generation of COx-free hydrogen via ammonia decomposition. Catalysis Today. 2011;164(1):112-8.

[39] Garbarino G, Bellotti D, Riani P, Magistri L, Busca G. Methanation of carbon dioxide on Ru/Al2O3 and Ni/Al2O3 catalysts at atmospheric pressure: Catalysts activation, behaviour and stability. International Journal of Hydrogen Energy. 2015;40(30):9171-82.

[40] Stangeland K, Kalai D, Li H, Yu Z. CO2 Methanation: The Effect of Catalysts and Reaction Conditions. Energy Procedia. 2017;105:2022-7.

[41] Wender I. Reactions of synthesis gas. Fuel Processing Technology. 1996;48(3):189-297.

[42] Jürgensen L, Ehimen EA, Born J, Holm-Nielsen JB. Dynamic biogas upgrading based on the Sabatier process: Thermodynamic and dynamic process simulation. Bioresource Technology. 2015;178:323-9.

[43] Hermesmann M, Grübel K, Scherotzki L, Müller TE. Promising pathways: The geographic and energetic potential of power-to-x technologies based on regeneratively obtained hydrogen. Renewable and Sustainable Energy Reviews. 2021;138:110644.

[44] Gebauer-Henke E, Blumenthal L, Prokofieva A, Vogt H, Voss G, Müller TE. Diastereomer control in the hydrogenation of o- and p-toluidine over ruthenium catalysts. Al'ternativnaya Energetika i Ekologiya. 2010(4):29-36.

[45] Tomkins P, Müller TE. Enhanced Selectivity in the Hydrogenation of Anilines to Cyclo-aliphatic Primary Amines over Lithium-Modified Ru/CNT Catalysts. ChemCatChem. 2018;10(6):1438-45.

[46] Kraynov A, Gebauer-Henke E, Leitner W, Müller TE. Unexpectedly high catalytic activity of ruthenium catalysts in the hydrogenation of nitrobenzene. Al'ternativnaya Energetika i Ekologiya. 2010;4:37-44.

[47] Gebauer-Henke E, Tomkins P, Leitner W, Müller TE. Nitro Promoters for Selectivity Control in the Core Hydrogenation of Toluidines: Controlling Adsorption on Catalyst Surfaces. ChemCatChem. 2014;6(10):2910-7.

[48] Tomkins P, Gebauer-Henke E, Leitner W, Müller TE. Concurrent Hydrogenation of Aromatic and Nitro Groups over Carbon-Supported Ruthenium Catalysts. ACS Catalysis. 2015;5(1):203-9.

[49] Almithn A, Hibbitts D. Comparing Rate and Mechanism of Ethane

Hydrogenolysis on Transition-Metal Catalysts. The Journal of Physical Chemistry C. 2019;123(9):5421-32.

[50] Morris RH. Physical insights into mechanistic processes in organometallic chemistry: an introduction. Faraday Discussions. 2019;220(0):10-27.

[51] Morris RH. Moving Hydrogen Using Iron Catalysts. Preprints of Papers-American Chemical Society, Division of Energy & Fuels. 2013;58(1):694-5.

[52] Václavík J, Kačer P, Kuzma M, Červený L. Opportunities Offered by Chiral η6-Arene/N-Arylsulfonyl-diamine-RuII Catalysts in the Asymmetric Transfer Hydrogenation of Ketones and Imines. Molecules. 2011;16(7):5460-95.

[53] Pan Y, Luo Z, Xu X, Zhao H, Han J, Xu L, et al. Ru-Catalyzed Deoxygenative Transfer Hydrogenation of Amides to Amines with Formic Acid/Triethylamine. Advanced Synthesis & Catalysis. 2019;361(16):3800-6.

[54] Labes R, González-Calderón D, Battilocchio C, Mateos C, Cumming GR, de Frutos O, et al. Rapid Continuous Ruthenium-Catalysed Transfer Hydrogenation of Aromatic Nitriles to Primary Amines. Synlett. 2017;28(20):2855-8.

[55] Cotman AE. Escaping from Flatland: Stereoconvergent Synthesis of Three-Dimensional Scaffolds via Ruthenium(II)-Catalyzed Noyori–Ikariya Transfer Hydrogenation. Chemistry – A European Journal. 2021;27(1):39-53.

[56] Ikariya T, Murata K, Noyori R. Bifunctional transition metal-based molecular catalysts for asymmetric syntheses. Organic & Biomolecular Chemistry. 2006;4(3):393-406.

[57] Grubbs RH, Trnka TM. Ruthenium-Catalyzed Olefin Metathesis. Ruthenium in Organic Synthesis. 2004:153-77.

[58] Beligny S, Blechert S. N-Heterocyclic Carbene–Ruthenium Complexes in Olefin Metathesis. In: Nolan SP, editor. N-Heterocyclic Carbenes in Synthesis. Weinheim: Wiley-VCH; 2006. p. 1-25.

[59] Schmidt B. Ruthenium-Catalyzed Cyclizations: More than Just Olefin Metathesis! Angewandte Chemie International Edition. 2003;42(41):4996-9.

[60] Hey DA, Reich RM, Baratta W, Kühn FE. Current advances on ruthenium(II) N-heterocyclic carbenes in hydrogenation reactions. Coordination Chemistry Reviews. 2018;374:114-32.

[61] Burling S, Paine BM, Whittlesey MK. Ruthenium N-Heterocyclic Carbene Complexes in Organic Transformations (Excluding Metathesis). In: Nolan SP, editor. N-Heterocyclic Carbenes in Synthesis. Weinheim: Wiley-VCH; 2006. p. 27-53.

[62] Nishikawa T, Kamigaito M, Sawamoto M. Living Radical Polymerization in Water and Alcohols: Suspension Polymerization of Methyl Methacrylate with RuCl2(PPh3)3 Complex. Macromolecules. 1999;32(7):2204-9.

[63] Ando T, Sawauchi C, Ouchi M, Kamigaito M, Sawamoto M. Amino alcohol additives for the fast living radical polymerization of methyl methacrylate with RuCl2(PPh3)3. Journal of Polymer Science Part A: Polymer Chemistry. 2003;41(22):3597-605.

[64] Hamasaki S, Kamigaito M, Sawamoto M. Amine Additives for Fast Living Radical Polymerization of Methyl Methacrylate with RuCl2(PPh3)3. Macromolecules. 2002;35(8):2934-40.

[65] Nieuwenhuys BE. Adsorption and Reactions of CO, NO, H2 and O2 on Group VIII Metal Surfaces. In: Joyner RW, van Santen RA, editors. Elementary Reaction Steps in Heterogeneous Catalysis. Dordrecht: Springer Netherlands; 1993. p. 155-77.

[66] Puisto M, Nenonen H, Puisto A, Alatalo M. Effect of van der Waals interactions on H2 dissociation on clean and defected Ru(0001) surface. The European Physical Journal B. 2013;86(9):396.

[67] Luppi M, Olsen RA, Baerends EJ. Six-dimensional potential energy surface for H2 at Ru(0001). Physical Chemistry Chemical Physics. 2006;8(6):688-96.

[68] Gutmann T, del Rosal I, Chaudret B, Poteau R, Limbach H-H, Buntkowsky G. From Molecular Complexes to Complex Metallic Nanostructures—2H Solid-State NMR Studies of Ruthenium-Containing Hydrogenation Catalysts. ChemPhysChem. 2013;14(13):3026-33.

[69] García-García FR, Bion N, Duprez D, Rodríguez-Ramos I, Guerrero-Ruiz A. H2/D2 isotopic exchange: A tool to characterize complex hydrogen interaction with carbon-supported ruthenium catalysts. Catalysis Today. 2016;259:9-18.

[70] Walaszek B, Yeping X, Adamczyk A, Breitzke H, Pelzer K, Limbach H-H, et al. 2H-solid-state-NMR study of hydrogen adsorbed on catalytically active ruthenium coated mesoporous silica materials. Solid State Nuclear Magnetic Resonance. 2009;35(3):164-71.

[71] Scholten JJF, Pijpers AP, Hustings AML. Surface Characterization of Supported and Nonsupported Hydrogenation Catalysts. Catalysis Reviews. 1985;27(1):151-206.

[72] Groß A. Theoretical Surface Science. 2 ed. Berlin Heidelberg: Springer-Verlag; 2009. XIII, 342 p.

[73] Vattuone L, Savio L, Rocca M. Bridging the structure gap: Chemistry of nanostructured surfaces at well-defined defects. Surface Science Reports. 2008;63(3):101-68.

[74] Zupanc C, Hornung A, Hinrichsen O, Muhler M. The Interaction of Hydrogen with Ru/MgO Catalysts. Journal of Catalysis. 2002;209(2):501-14.

[75] Vayssilov GN, Petrova GP, Shor EAI, Nasluzov VA, Shor AM, Petkov PS, et al. Reverse hydrogen spillover on and hydrogenation of supported metal clusters: insights from computational model studies. Physical Chemistry Chemical Physics. 2012;14(17):5879-90.

[76] Swart I, de Groot FMF, Weckhuysen BM, Gruene P, Meijer G, Fielicke A. H2 Adsorption on 3d Transition Metal Clusters: A Combined Infrared Spectroscopy and Density Functional Study. The Journal of Physical Chemistry A. 2008;112(6):1139-49.

[77] Nordlander P, Holloway S, Nørskov JK. Hydrogen adsorption on metal surfaces. Surface Science. 1984;136(1):59-81.

[78] Faglioni F, Goddard WA. Energetics of hydrogen coverage on group VIII transition metal surfaces and a kinetic model for adsorption/desorption. The Journal of Chemical Physics. 2004;122(1):014704.

[79] Bhatia S, Engelke F, Pruski M, Gerstein BC, King TS. Interaction of Hydrogen with Supported Ru Catalysts: High Pressure in Situ NMR Studies. Journal of Catalysis. 1994;147(2):455-64.

[80] Berthoud R, Délichère P, Gajan D, Lukens W, Pelzer K, Basset J-M, et al. Hydrogen and oxygen adsorption stoichiometries on silica supported ruthenium nanoparticles. Journal of Catalysis. 2008;260(2):387-91.

[81] Peden CHF, Goodman DW, Houston JE, Yates JT. Subsurface hydrogen on Ru(0001): Quantification by Cu titration. Surface Science. 1988;194(1):92-100.

[82] Almithn A, Hibbitts D. Effects of Catalyst Model and High Adsorbate Coverages in ab Initio Studies of Alkane Hydrogenolysis. ACS Catalysis. 2018;8(7):6375-87.

[83] Liu J, Hibbitts D, Iglesia E. Dense CO Adlayers as Enablers of CO Hydrogenation Turnovers on Ru Surfaces. Journal of the American Chemical Society. 2017;139(34):11789-802.

[84] Lechner BAJ, Feng X, Feibelman PJ, Cerdá JI, Salmeron M. Scanning Tunneling Microscopy Study of the Structure and Interaction between Carbon Monoxide and Hydrogen on the Ru(0001) Surface. The Journal of Physical Chemistry B. 2018;122(2):649-56.

[85] Makgabutlane B, Nthunya LN, Maubane-Nkadimeng MS, Mhlanga SD. Green synthesis of carbon nanotubes to address the water-energy-food nexus: A critical review. Journal of Environmental Chemical Engineering. 2020;9(1):104736.

[86] Omoriyekomwan JE, Tahmasebi A, Dou J, Wang R, Yu J. A review on the recent advances in the production of carbon nanotubes and carbon nanofibers via microwave-assisted pyrolysis of biomass. Fuel Processing Technology. 2020;214:106686.

[87] Müller TE, Reid DG, Hsu WK, Hare JP, Kroto HW, Walton DRM. Synthesis of nanotubes via catalytic pyrolysis of acetylene: A SEM study. Carbon. 1997;35(7):951-66.

[88] Reddy CK, Priya L, Saikumari G. Carbon nano tubes. Eur J Biomed Pharm Sci. 2019;6(13):201-4.

[89] Soni SK, Thomas B, Kar VR. A Comprehensive Review on CNTs and CNT-Reinforced Composites: Syntheses, Characteristics and Applications. Materials Today Communications. 2020;25:101546.

[90] Esteves LM, Oliveira HA, Passos FB. Carbon nanotubes as catalyst support in chemical vapor deposition reaction: A review. Journal of Industrial and Engineering Chemistry. 2018;65:1-12.

[91] Datsyuk V, Kalyva M, Papagelis K, Parthenios J, Tasis D, Siokou A, et al. Chemical oxidation of multiwalled carbon nanotubes. Carbon. 2008;46(6):833-40.

[92] Database of Zeolite Structures [Internet]. [cited 30.12.2020]. Available from: http://www.iza-structure.org/databases/.

[93] Jana SK, Mochizuki A, Namba S. Progress in Pore-Size Control of Mesoporous MCM-41 Molecular Sieve Using Surfactant Having Different Alkyl Chain Lengths and Various Organic Auxiliary Chemicals. Catalysis Surveys from Asia. 2004;8(1):1-13.

[94] Kraynov A, Müller TE. Concepts for the Stabilization of Metal Nanoparticles in Ionic Liquids. In: Scott, editor. Applications of Ionic Liquids in Science and Technology. 9. Tennessee: InTech; 2011. p. 235-60.

[95] Schmid G, editor. At the boundary of the metallic state. 1996: Vieweg.

[96] Gu Y, Li G. Ionic Liquids-Based Catalysis with Solids: State of the Art. Advanced Synthesis & Catalysis. 2009;351(6):817-47.

[97] Meijboom R, Haumann M, Müller TE, Szesni N. Synthetic methodologies for supported ionic liquid materials. In: Fehrmann R, Riisager A, Haumann M, editors. Supported Ionic

Liquids. Weinheim: Wiley-VCH Verlag GmbH & Co. KGaA; 2014. p. 75-93.

[98] Sievers C, Jimenez O, Müller TE, Steuernagel S, Lercher JA. Formation of Solvent Cages around Organometallic Complexes in Thin Films of Supported Ionic Liquid. Journal of the American Chemical Society. 2006;128(43):13990-1.

[99] Müller TE. Supported Ionic Liquids as Part of a Building-Block System for Tailored Catalysts. Supported Ionic Liquids. Wiley Online Books. Weinheim: Wiley-VCH Verlag GmbH & Co. KGaA; 2014. p. 209-32.

[100] Jimenez O, Müller TE, Lercher JA. Tailoring Adsorption—Desorption Properties of Hydroamination Catalysts with Ionic Liquids. Ionic Liquids in Organic Synthesis. ACS Symposium Series. 950: American Chemical Society; 2007. p. 267-80.

[101] Fow KL, Jaenicke S, Müller TE, Sievers C. Enhanced enantioselectivity of chiral hydrogenation catalysts after immobilisation in thin films of ionic liquid. Journal of Molecular Catalysis A: Chemical. 2008;279(2):239-47.

[102] Goldstein IS. Chemicals from cellulose. In Goldstein IS, editor. Organic chemicals from biomass. Boca Raton: CRC Press; 1981. p. 101-24.

[103] Okada K, Fujiwara S, Tsuzuki M. Energy conservation in photosynthetic microorganisms. The Journal of General and Applied Microbiology. 2020;66(2):59-65.

[104] Ragauskas AJ, Williams CK, Davison BH, Britovsek G, Cairney J, Eckert CA, et al. The Path Forward for Biofuels and Biomaterials. Science. 2006;311(5760):484.

[105] Kamm B, Gruber PR, Kamm M. Biorefineries-industrial processes and products. Weinheim: Wiley-VCH; 2016.

[106] Louarn G, Lecoeur J, Lebon E. A Three-dimensional Statistical Reconstruction Model of Grapevine (*Vitis vinifera*) Simulating Canopy Structure Variability within and between Cultivar/Training System Pairs. Annals of Botany. 2008;101(8):1167-84.

[107] Vargas LA, Andersen MN, Jensen CR, Jørgensen U. Estimation of leaf area index, light interception and biomass accumulation of *Miscanthus sinensis* 'Goliath' from radiation measurements. Biomass and Bioenergy. 2002;22(1):1-14.

[108] Bai Z, Mao S, Han Y, Feng L, Wang G, Yang B, et al. Study on Light Interception and Biomass Production of Different Cotton Cultivars. PLOS ONE. 2016;11(5):e0156335.

[109] Rinaldi R, Schüth F. Design of solid catalysts for the conversion of biomass. Energy & Environmental Science. 2009;2(6):610-26.

[110] Laskar DD, Yang B, Wang H, Lee J. Pathways for biomass-derived lignin to hydrocarbon fuels. Biofuels, Bioproducts and Biorefining. 2013;7(5):602-26.

[111] Hoekman SK, Broch A, Robbins C, Ceniceros E, Natarajan M. Review of biodiesel composition, properties, and specifications. Renewable and Sustainable Energy Reviews. 2012;16(1):143-69.

[112] Dorrestijn E, Laarhoven LJJ, Arends IWCE, Mulder P. The occurrence and reactivity of phenoxyl linkages in lignin and low rank coal. Journal of Analytical and Applied Pyrolysis. 2000;54(1):153-92.

[113] BabeŁ K, Janasiak D, Waliszewska B, PrĄDzyŃSki W. Chemical composition of lignocellulose materials and porous structure of activated carbons. Annals of Warsaw University of Life Sciences-SGGW,

Forestry and Wood Technology. 2012;77:33-40.

[114] Figueiras FG, Fraga F, Pérez FF, Ríos AF. Theoretical limits of oxygen:carbon and oxygen:nitrogen ratios during photosynthesis and mineralisation of organic matter in the sea. Scientia Marina. 1998;62(1-2):161-8.

[115] Moore TR, Large D, Talbot J, Wang M, Riley JL. The Stoichiometry of Carbon, Hydrogen, and Oxygen in Peat. Journal of Geophysical Research: Biogeosciences. 2018;123(10):3101-10.

[116] Strel'nikova EB, Goncharov IV, Serebrennikova OV. Concentration and distribution of oxygen-containing compounds in crude oils from the southeastern part of Western Siberia. Petroleum Chemistry. 2012;52(4):278-83.

[117] Guo K, Zhang Y, Shi Q, Yu Z. The Effect of Carbon-Supported Nickel Nanoparticles in the Reduction of Carboxylic Acids for in Situ Upgrading of Heavy Crude Oil. Energy & Fuels. 2017;31(6):6045-55.

[118] Wagemann, K. et al. Roadmap Bioraffinerien. Berlin: Bundesministerium für Ernährung, Landwirtschaft und Verbraucherschutz (BMELV), Bundesministerium für Bildung und Forschung (BMBF), Bundesministerium für Umwelt, Naturschutz und Reaktorsicherheit (BMU), Bundesministerium für Wirtschaft undEnergie (BMWi); 2014.

[119] Chaturvedi T, Torres AI, Stephanopoulos G, Thomsen MH, Schmidt JE. Developing Process Designs for Biorefineries—Definitions, Categories, and Unit Operations. Energies. 2020;13(6):1493.

[120] Sheldon RA. Biocatalysis and Green Chemistry. In: Patel, RN, editor. Green Biocatalysis. Hoboken: Wiley & Sons Ltd; 2016:1-15.

[121] Sjostrom E. Wood chemistry: fundamentals and applications. London: Academic Press; 2013. 293 p.

[122] Sun L, Vella P, Schnell R, Polyakova A, Bourenkov G, Li F, et al. Structural and Functional Characterization of the BcsG Subunit of the Cellulose Synthase in Salmonella typhimurium. Journal of Molecular Biology. 2018;430(18, Part B):3170-89.

[123] Yang P, Kobayashi H, Fukuoka A. Recent Developments in the Catalytic Conversion of Cellulose into Valuable Chemicals. Chinese Journal of Catalysis. 2011;32(5):716-22.

[124] Pontes MH, Lee E-J, Choi J, Groisman EA. Salmonella promotes virulence by repressing cellulose production. Proceedings of the National Academy of Sciences. 2015;112(16):5183.

[125] Li S, Bashline L, Lei L, Gu Y. Cellulose synthesis and its regulation. Arabidopsis Book. 2014;12:e0169-e.

[126] Berglund J, Angles d'Ortoli T, Vilaplana F, Widmalm G, Bergenstråhle-Wohlert M, Lawoko M, et al. A molecular dynamics study of the effect of glycosidic linkage type in the hemicellulose backbone on the molecular chain flexibility. The Plant Journal. 2016;88(1):56-70.

[127] Schulze M, Bergs M, Monakhova Y, Diehl B, Konow C, Völkering G, et al. Lignins Isolated via Catalyst-free Organosolv Pulping from Miscanthus x giganteus, *M. sinensis*, *M. robustus* and M. nagara: A Comparative Study. Preprints 2021:2021010181.

[128] Crestini C, Melone F, Sette M, Saladino R. Milled Wood Lignin: A Linear Oligomer. Biomacromolecules. 2011;12(11):3928-35.

[129] Song B, Lin R, Lam CH, Wu H, Tsui T-H, Yu Y. Recent advances and challenges of inter-disciplinary

biomass valorization by integrating hydrothermal and biological techniques. Renewable and Sustainable Energy Reviews. 2021;135:110370.

[130] Hiras J, Wu Y-W, Deng K, Nicora CD, Aldrich JT, Frey D, et al. Comparative Community Proteomics Demonstrates the Unexpected Importance of Actinobacterial Glycoside Hydrolase Family 12 Protein for Crystalline Cellulose Hydrolysis. mBio. 2016;7(4):e01106-16.

[131] Solarte-Toro JC, González-Aguirre JA, Poveda Giraldo JA, Cardona Alzate CA. Thermochemical processing of woody biomass: A review focused on energy-driven applications and catalytic upgrading. Renewable and Sustainable Energy Reviews. 2021;136:110376.

[132] Morales G, Iglesias J, Melero JA. Sustainable catalytic conversion of biomass for the production of biofuels and bioproducts. Catalysts. 2020;10(5):581.

[133] Li W, Wanninayake N, Gao X, Li M, Pu Y, Kim D-Y, et al. Mechanistic Insight into Lignin Slow Pyrolysis by Linking Pyrolysis Chemistry and Carbon Material Properties. ACS Sustainable Chemistry & Engineering. 2020;8(42):15843-54.

[134] Ghysels S, Dubuisson B, Pala M, Rohrbach L, Van den Bulcke J, Heeres HJ, et al. Improving fast pyrolysis of lignin using three additives with different modes of action. Green Chemistry. 2020;22(19):6471-88.

[135] Terrell E, Dellon LD, Dufour A, Bartolomei E, Broadbelt LJ, Garcia-Perez M. A Review on Lignin Liquefaction: Advanced Characterization of Structure and Microkinetic Modeling. Industrial & Engineering Chemistry Research. 2020;59(2):526-55.

[136] Kawamoto H, Horigoshi S, Saka S. Pyrolysis reactions of various lignin model dimers. Journal of Wood Science. 2007;53(2):168-74.

[137] Dionisi D, Anderson JA, Aulenta F, McCue A, Paton G. The potential of microbial processes for lignocellulosic biomass conversion to ethanol: a review. Journal of Chemical Technology & Biotechnology. 2015;90(3):366-83.

[138] Zeng Y, Zhao S, Yang S, Ding S-Y. Lignin plays a negative role in the biochemical process for producing lignocellulosic biofuels. Current Opinion in Biotechnology. 2014;27:38-45.

[139] Beauchet R, Monteil-Rivera F, Lavoie JM. Conversion of lignin to aromatic-based chemicals (L-chems) and biofuels (L-fuels). Bioresource Technology. 2012;121:328-34.

[140] Evstigneyev EI, Shevchenko SM. Lignin valorization and cleavage of arylether bonds in chemical processing of wood: a mini-review. Wood Science and Technology. 2020;54(4):787-820.

[141] Margellou A, Triantafyllidis KS. Catalytic Transfer Hydrogenolysis Reactions for Lignin Valorization to Fuels and Chemicals. Catalysts. 2019;9(1):43.

[142] Jing Y, Dong L, Guo Y, Liu X, Wang Y. Chemicals from Lignin: A Review of Catalytic Conversion Involving Hydrogen. ChemSusChem. 2020;13(17):4181-98.

[143] Chen X, Guan W, Tsang C-W, Hu H, Liang C. Lignin Valorizations with Ni Catalysts for Renewable Chemicals and Fuels Productions. Catalysts. 2019;9(6):488.

[144] Wang L, Zhang J, Yi X, Zheng A, Deng F, Chen C, et al. Mesoporous ZSM-5 Zeolite-Supported Ru Nanoparticles as Highly Efficient

Catalysts for Upgrading Phenolic Biomolecules. ACS Catalysis. 2015;5(5):2727-34.

[145] Fiorani G, Crestini C, Selva M, Perosa A. Advancements and Complexities in the Conversion of Lignocellulose Into Chemicals and Materials. Frontiers in Chemistry. 2020;8:797.

[146] Mishra DK, Dabbawala AA, Park JJ, Jhung SH, Hwang J-S. Selective hydrogenation of d-glucose to d-sorbitol over HY zeolite supported ruthenium nanoparticles catalysts. Catalysis Today. 2014;232:99-107.

[147] Ziolkowska JR. Chapter 1 - Biofuels technologies: An overview of feedstocks, processes, and technologies. In: Ren J, Scipioni A, Manzardo A, Liang H, editors. Biofuels for a More Sustainable Future. Amsterdam: Elsevier; 2020. p. 1-19.

[148] Li C, Xu G, Wang C, Ma L, Qiao Y, Zhang Y, et al. One-pot chemocatalytic transformation of cellulose to ethanol over Ru-WOx/HZSM-5. Green Chem. 2019;21(9):2234-9.

[149] Manaenkov OV, Kislitza OV, Filatova AE, Doluda VY, Sulman EM, Sidorov AI, et al. Cellulose conversion to polyols in subcritical water. Russian Journal of Physical Chemistry B. 2016;10(7):1116-22.

[150] Matveeva VG, Sulman EM, Manaenkov OV, Filatova AE, Kislitza OV, Sidorov AI, et al. Hydrolytic hydrogenation of cellulose in subcritical water with the use of the Ru-containing polymeric catalysts. Catalysis Today. 2017;280:45-50.

[151] Dabbawala AA, Mishra DK, Hwang J-S. Selective hydrogenation of D-glucose using amine functionalized nanoporous polymer supported Ru nanoparticles based catalyst. Catalysis Today. 2016;265:163-73.

[152] Martinuzzi S, Cozzula D, Centomo P, Zecca M, Müller TE. The distinct role of the flexible polymer matrix in catalytic conversions over immobilised nanoparticles. RSC Advances. 2015;5(69):56181-8.

[153] Rey-Raap N, Ribeiro LS, Orfao JJdM, Figueiredo JL, Pereira MFR. Catalytic conversion of cellulose to sorbitol over Ru supported on biomass-derived carbon-based materials. Applied Catalysis B: Environmental. 2019;256:117826.

[154] S. Ribeiro L, Órfão JJM, R. Pereira MF. Enhanced direct production of sorbitol by cellulose ball-milling. Green Chemistry. 2015;17(5):2973-80.

[155] Ribeiro LS, Delgado JJ, de Melo Órfão JJ, Pereira MFR. Direct conversion of cellulose to sorbitol over ruthenium catalysts: Influence of the support. Catalysis Today. 2017;279:244-51.

[156] Song Z, Wang H, Niu Y, Liu X, Han J. Selective conversion of cellulose to hexitols over bi-functional Ru-supported sulfated zirconia and silica-zirconia catalysts. Frontiers of Chemical Science and Engineering. 2015;9(4):461-6.

[157] Guo X, Wang X, Guan J, Chen X, Qin Z, Mu X, et al. Selective hydrogenation of D-glucose to D-sorbitol over Ru/ZSM-5 catalysts. Chinese Journal of Catalysis. 2014;35(5):733-40.

[158] Wang S, Wei W, Zhao Y, Li H, Li H. Ru–B amorphous alloy deposited on mesoporous silica nanospheres: An efficient catalyst for D-glucose hydrogenation to D-sorbitol. Catalysis Today. 2015;258:327-36.

[159] Guo X, Guan J, Li B, Wang X, Mu X, Liu H. Conversion of biomass-derived sorbitol to glycols over carbon-materials supported Ru-based catalysts. Scientific Reports. 2015;5:16451pp.

[160] Bouxin FP, Strub H, Dutta T, Aguilhon J, Morgan TJ, Mingardon F, et al. Elucidating transfer hydrogenation mechanisms in non-catalytic lignin depolymerization. Green Chemistry. 2018;20(15):3566-80.

[161] Wu H, Song J, Xie C, Wu C, Chen C, Han B. Efficient and Mild Transfer Hydrogenolytic Cleavage of Aromatic Ether Bonds in Lignin-Derived Compounds over Ru/C. ACS Sustainable Chemistry & Engineering. 2018;6(3):2872-7.

[162] Petrus L, Noordermeer MA. Biomass to biofuels, a chemical perspective. Green Chemistry. 2006;8(10):861-7.

[163] Kalinoski RM, Li W, Mobley JK, Asare SO, Dorrani M, Lynn BC, et al. Antimicrobial Properties of Corn Stover Lignin Fractions Derived from Catalytic Transfer Hydrogenolysis in Supercritical Ethanol with a Ru/C Catalyst. ACS Sustainable Chemistry & Engineering. 2020;8(50):18455-67.

[164] Shirai M, Osada M, Yamaguchi A, Hiyoshi N, Sato O. Chapter 15 - Utilization of Supercritical Fluid for Catalytic Thermochemical Conversions of Woody-Biomass Related Compounds. In: Pandey A, Bhaskar T, Stöcker M, Sukumaran RK, editors. Recent Advances in Thermo-Chemical Conversion of Biomass. Boston: Elsevier; 2015. p. 437-53.

[165] Müller TE, Mingos DMP. Determination of the Tolman cone angle from crystallographic parameters and a statistical analysis using the crystallographic data base. Transition Metal Chemistry. 1995;20(6):533-9.

[166] Batsanov SS. Van der Waals Radii of Hydrogen in Gas-Phase and Condensed Molecules. Structural Chemistry. 1999;10(6):395-400.